Molecular Cell

Article

Centromere/kinetochore is assembled through CENP-C oligomerization

Graphical abstract

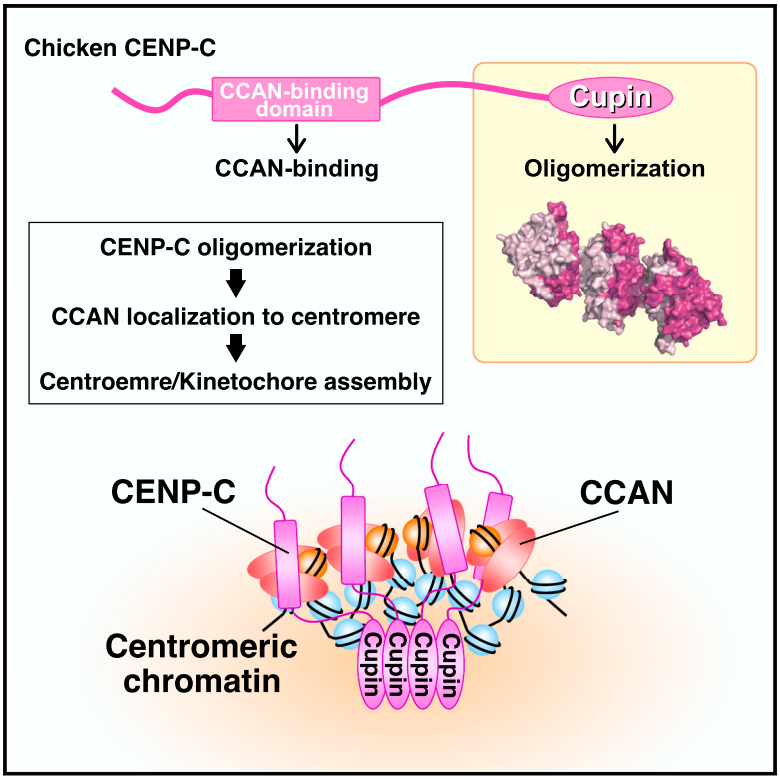

Highlights

- CENP-C domains that are required and sufficient for its function are defined
- CENP-C is oligomerized through the Cupin domain and its extended region
- CENP-C oligomerization is required for cell viability and mitotic progression
- CENP-C oligomerization is crucial for centromere/kinetochore assembly

Authors

Masatoshi Hara, Mariko Ariyoshi, Tomoki Sano, ..., Isabelle Jansen, Toru Hirota, Tatsuo Fukagawa

Correspondence

mahara@fbs.osaka-u.ac.jp (M.H.), fukagawa.tatsuo.fbs@osaka-u.ac.jp (T.F.)

In brief

Hara et al. find that CENP-C, a centromeric protein, is oligomerized through the Cupin domain in its C-terminal region. The oligomerization of the Cupin domain is essential for CENP-C function to localize CCAN proteins to centromeres and assemble kinetochore and centromeric chromatin.

Hara et al., 2023, Molecular Cell *83*, 2188–2205
July 6, 2023
https://doi.org/10.1016/j.molcel.2023.05.023

CellPress

CellPress
OPEN ACCESS

Molecular Cell

Article

Centromere/kinetochore is assembled through CENP-C oligomerization

Masatoshi Hara,[1,*] Mariko Ariyoshi,[1] Tomoki Sano,[1] Ryu-Suke Nozawa,[2] Soya Shinkai,[3] Shuichi Onami,[3] Isabelle Jansen,[4] Toru Hirota,[2] and Tatsuo Fukagawa[1,5,*]

[1]Graduate School of Frontier Biosciences, Osaka University, Suita, Osaka 565-0871, Japan
[2]Division of Experimental Pathology, Cancer Institute of the Japanese Foundation for Cancer Research, Tokyo 135-8550, Japan
[3]Laboratory for Developmental Dynamics, RIKEN Center for Biosystems Dynamics Research, Kobe 650-0047, Japan
[4]Abberior Instruments GmbH, Göttingen 37077, Germany
[5]Lead contact
*Correspondence: mahara@fbs.osaka-u.ac.jp (M.H.), fukagawa.tatsuo.fbs@osaka-u.ac.jp (T.F.)
https://doi.org/10.1016/j.molcel.2023.05.023

SUMMARY

Kinetochore is an essential protein complex required for accurate chromosome segregation. The constitutive centromere-associated network (CCAN), a subcomplex of the kinetochore, associates with centromeric chromatin and provides a platform for the kinetochore assembly. The CCAN protein CENP-C is thought to be a central hub for the centromere/kinetochore organization. However, the role of CENP-C in CCAN assembly needs to be elucidated. Here, we demonstrate that both the CCAN-binding domain and the C-terminal region that includes the Cupin domain of CENP-C are necessary and sufficient for chicken CENP-C function. Structural and biochemical analyses reveal self-oligomerization of the Cupin domains of chicken and human CENP-C. We find that the CENP-C Cupin domain oligomerization is vital for CENP-C function, centromeric localization of CCAN, and centromeric chromatin organization. These results suggest that CENP-C facilitates the centromere/kinetochore assembly through its oligomerization.

INTRODUCTION

The kinetochore is a large protein complex, which is essential for accurate chromosome segregation during mitosis and meiosis. The kinetochore structure includes two major complexes: the constitutive centromere-associated network (CCAN) and the KMN (KNL1, Mis12, and Ndc80 complexes) network.[1–5] In vertebrates, CCAN is represented by a 16-protein complex that recognizes the centromeric chromatin containing the histone H3 variant CENP-A and constitutively localizes to the centromere throughout the cell cycle.[6–14] During the late G2 and M phases, CCAN provides a binding platform for the KMN network, which directly binds to spindle microtubules linking the centromeric chromatin to spindle microtubules.[2,3,15–19]

Extensive in vitro studies and structural analyses have revealed that the CCAN proteins form several subcomplexes that assemble the CCAN through multivalent interactions.[13,20–25] Recent cryo-electron microscopic analyses have proposed structural models of CCAN associated with the CENP-A nucleosome. These models provide insights into the molecular organization of a CCAN unit binding to centromeric chromatin.[26,27] However, in these CCAN models, a large part of CENP-C, a CCAN protein, was not mapped due to its disordered characteristics. Moreover, the C-terminal region was truncated in the recombinant CENP-C used for CCAN reconstruction.[26,27] Therefore, the role of CENP-C in CCAN remains unclear.

CENP-C is essential for chromosome segregation and cell viability and is conserved among most model species belonging to various groups ranging from yeasts to human.[28–33] CENP-C, as a hub for kinetochore assembly, binds to various proteins associated with centromere/kinetochore through multiple functional domains.[34] Previously, we investigated two functional domains, the Mis12 complex (Mis12C)-binding and CENP-A nucleosome-binding domains (CENP-C motif), which were thought to be important for bridging centromeric chromatin with spindle microtubules during mitosis. However, these two domains were unexpectedly dispensable for CENP-C function in chicken DT40 cells.[35,36] The next questions to address are which domain(s) is crucial to CENP-C and what is the fundamental role(s) of CENP-C in CCAN.

In this study, we performed a genetic complementation assay using CENP-C conditional knockout chicken DT40 cells and identified the CCAN-binding domain (CBD) (PEST-rich domain), which binds to the CCAN subcomplexes,[20,23,26,27,34,37] and the C-terminal region including the Cupin domain, which was considered a homodimerization domain in yeasts and fly CENP-C homologs.[38–40] X-ray crystallographic and biochemical analyses revealed that the chicken and human CENP-C Cupin domain dimers were oligomerized. Furthermore, oligomerization

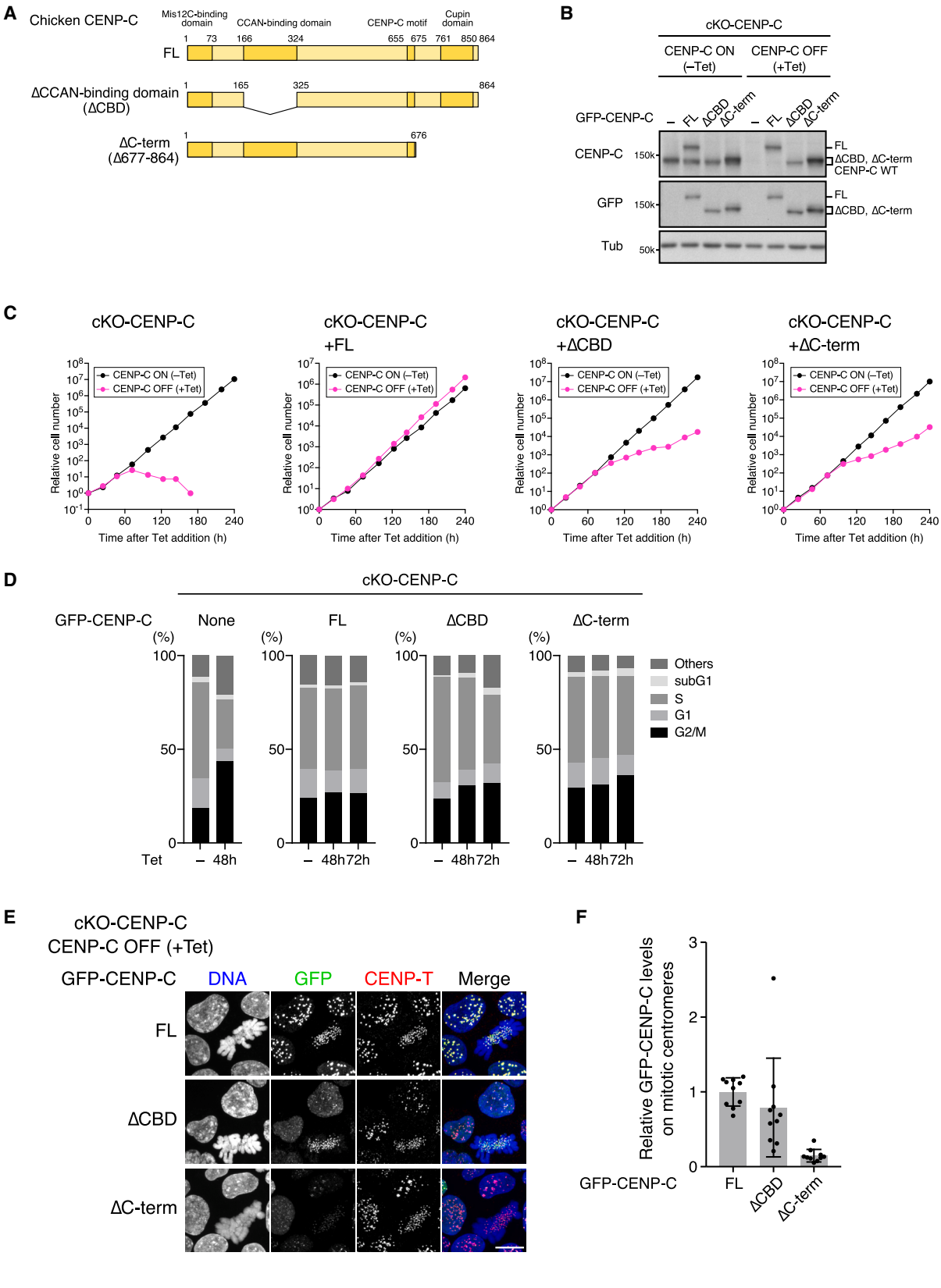

(legend on next page)

of the Cupin domain appeared to be essential for CENP-C function and centromeric localization, which is required for the stable localization of CCAN to the centromeres and maintenance of centromeric chromatin organization. These results suggest that CENP-C oligomerization induces the kinetochore/centromere assembly for accurate chromosome segregation.

RESULTS

CCAN-binding and Cupin domains of CENP-C are required for the CENP-C function

Chicken CENP-C contains four conserved domains (Figure 1A). Previously, we demonstrated that the Mis12C-binding domain and CENP-A nucleosome-binding domain (CENP-C motif) were dispensable for chicken DT40 cell viability and mitotic progression.[35,36] Considering the importance of CENP-C in DT40 cell viability and kinetochore function,[31,41] we analyzed the other two domains in chicken CENP-C to identify its functionally crucial domain(s): the domain binding to CCAN subcomplexes such as CENP-H-I-K-M and CENP-L-N subcomplexes (aa 166–324: CBD, PEST-rich domain in human CENP-C), and the Cupin domain (aa 761–850), known as a homodimerization domain present in yeasts and fruit fly CENP-C homologs[38–40] (Figure 1A).

We deleted the CBD or the C-terminal region (aa 677–864, C-term) that includes the Cupin domain from chicken CENP-C (CENP-C$^{\Delta CBD}$ or CENP-C$^{\Delta C\text{-term}}$) and expressed it as a GFP-fusion protein in CENP-C conditional knockout (cKO-CENP-C) DT40 cells. In cKO-CENP-C cells, wild-type CENP-C (CENP-C^{WT}) expression was turned off by a tetracycline (Tet) addition to the culture medium (Figure 1B). cKO-CENP-C cells, with no GFP-CENP-C expression, showed growth defects, including G2/M cell enrichment and cell death by 180 h after Tet addition (Figures 1C and 1D), which are attributable to erroneous chromosome loss due to kinetochore malfunction.[33] These growth and mitotic defects were suppressed by full-length CENP-C (CENP-C^{FL}) expression (Figures 1C and 1D). However, cKO-CENP-C cells expressing the CENP-C$^{\Delta CBD}$ or CENP-C$^{\Delta C\text{-term}}$ showed apparent albeit less growth deficiency and G2/M cell enrichment, demonstrating the importance of these domains for CENP-C function (Figures 1C and 1D).

Next, we examined the centromeric localization of the GFP-fused CENP-C mutants (Figures 1E and 1F). GFP-CENP-C^{FL} localized to centromeres labeled with CCAN protein CENP-T in both interphase and mitotic cells. Despite a minor reduction, GFP-CENP-C$^{\Delta CBD}$ localized to mitotic centromeres in Tet-treated cKO-CENP-C cells but diffused into the nuclei without evident centromeric localization in interphase cells (Figures 1E and 1F). CBD binds to CENP-H-I-K-M and CENP-L-N subcomplexes.[20,34,37] Previously, we observed CENP-H and CENP-K-dependent localization of CENP-C during interphase[41,42]; the reduction in the interphase centromeric localization of the CENP-C$^{\Delta CBD}$ was consistent with that outcome. During mitosis, CENP-C interacts with centromere through the CENP-C motif that binds to the CENP-A nucleosome in mitosis, but not in interphase,[36,43] explaining the mitotic localization of the CENP-C$^{\Delta CBD}$.

The GFP-CENP-C$^{\Delta C\text{-term}}$ signals at centromeres were strongly reduced in both interphase and mitotic Tet-treated cKO-CENP-C cells (Figures 1E and 1F), suggesting that the C-terminal region, including the Cupin domain, is crucial for centromeric localization of CENP-C through the CBD and CENP-C motif.

CCAN-binding and Cupin domains are sufficient for the CENP-C function

CENP-C contains a large flexible region.[34,44,45] In chicken CENP-C, its middle region (aa 325–654) was predicted to be disordered (Figure 2A). To test the involvement of this region in the CENP-C function, we deleted the disordered region and CENP-C motif, which is dispensable for chicken CENP-C function[36] (Δ325-676: ΔMid-DR) (Figure 2A). We expressed GFP-CENP-C$^{\Delta Mid\text{-}DR}$ in cKO-CENP-C cells and examined their growth (Figures 2B and 2C). CENP-C$^{\Delta Mid\text{-}DR}$ expression restored the growth defect observed in Tet-treated cKO-CENP-C cells, indicating that the middle-disordered region is dispensable for the CENP-C function (Figure 2C).

Furthermore, since the Mis12C-binding domain is also dispensable for chicken CENP-C function,[35] we removed the N terminus (aa 1–165) from the CENP-C$^{\Delta Mid\text{-}DR}$; this mutant contained only the CBD and C-terminal region (CENP-C$^{[166–324]\text{-}[677–864]}$). Strikingly, the CENP-C$^{[166–324]\text{-}[677–864]}$ restored the growth defects and G2/M enrichment in cKO-CENP-C cells, which suggests that the CENP-C$^{[166–324]\text{-}[677–864]}$ is functional (Figures 2A–2D). Additionally, truncated CENP-C with a further deletion in the C terminus (CENP-C$^{[166–324]\text{-}[722–864]}$) suppressed the CENP-C-deficient phenotypes (Figures 2A–2C). CENP-C$^{[166–324]\text{-}[677–864]}$ was used for further analyses as a minimal functional CENP-C in DT40 cells and was termed as "Mini-CENP-C" (Figure 2A).

In Tet-treated cKO-CENP-C cells, a low level of leaky CENP-C^{WT} expression in cKO-CENP-C cells, even after Tet addition, possibly supported the Mini-CENP-C-associated rescued CENP-C-deficient phenotypes. To ensure the sufficiency of Mini-CENP-C for CENP-C function in DT40 cells, we established endogenous CENP-C knockout (KO) cell lines expressing

Figure 1. CCAN-binding domain and C-terminal region including the Cupin domain are required for chicken CENP-C function in DT40 cells

(A) Schematic representation of chicken CENP-C (864 amino acids: CENP-C FL, NCBI Reference Sequence: NP_001376225.2). The CCAN-binding domain (aa 166–324, CBD) was deleted in CENP-C$^{\Delta CBD}$. The C terminus region, including the Cupin domain (aa 677–864, C-term), was deleted in CENP-C$^{\Delta C\text{-term}}$.

(B) GFP-fused CENP-C expression in CENP-C conditional knockout (cKO-CENP-C) chicken DT40 cells. GFP-fused CENP-C FL, ΔCBD, or ΔC-term was expressed in cKO-CENP-C cells in which wild-type CENP-C was conditionally knocked out by tetracycline (Tet) addition. The cells were cultured with or without Tet (+Tet or −Tet) for 48 h.

(C) Growth of cKO-CENP-C cells expressing GFP-CENP-C FL, ΔCBD, or ΔC-term. The cell numbers were normalized to those at 0 h for each line.

(D) Cell cycle in cKO-CENP-C cells expressing GFP-CENP-C FL, ΔCBD, or ΔC-term.

(E and F) GFP-CENP-C FL, ΔCBD, or ΔC-term localization in cKO-CENP-C cells. The cells were cultured as in (B). Scale bar, 10 μm. GFP-CENP-C signals on centromere in mitotic cells were quantified in (F). (Unpaired t test, two-tailed, mean ± SD, n = 10, FL vs. ΔCBD: ns ($p = 0.3480$), FL vs. ΔC-term: $p < 0.0001$).

CellPress
OPEN ACCESS

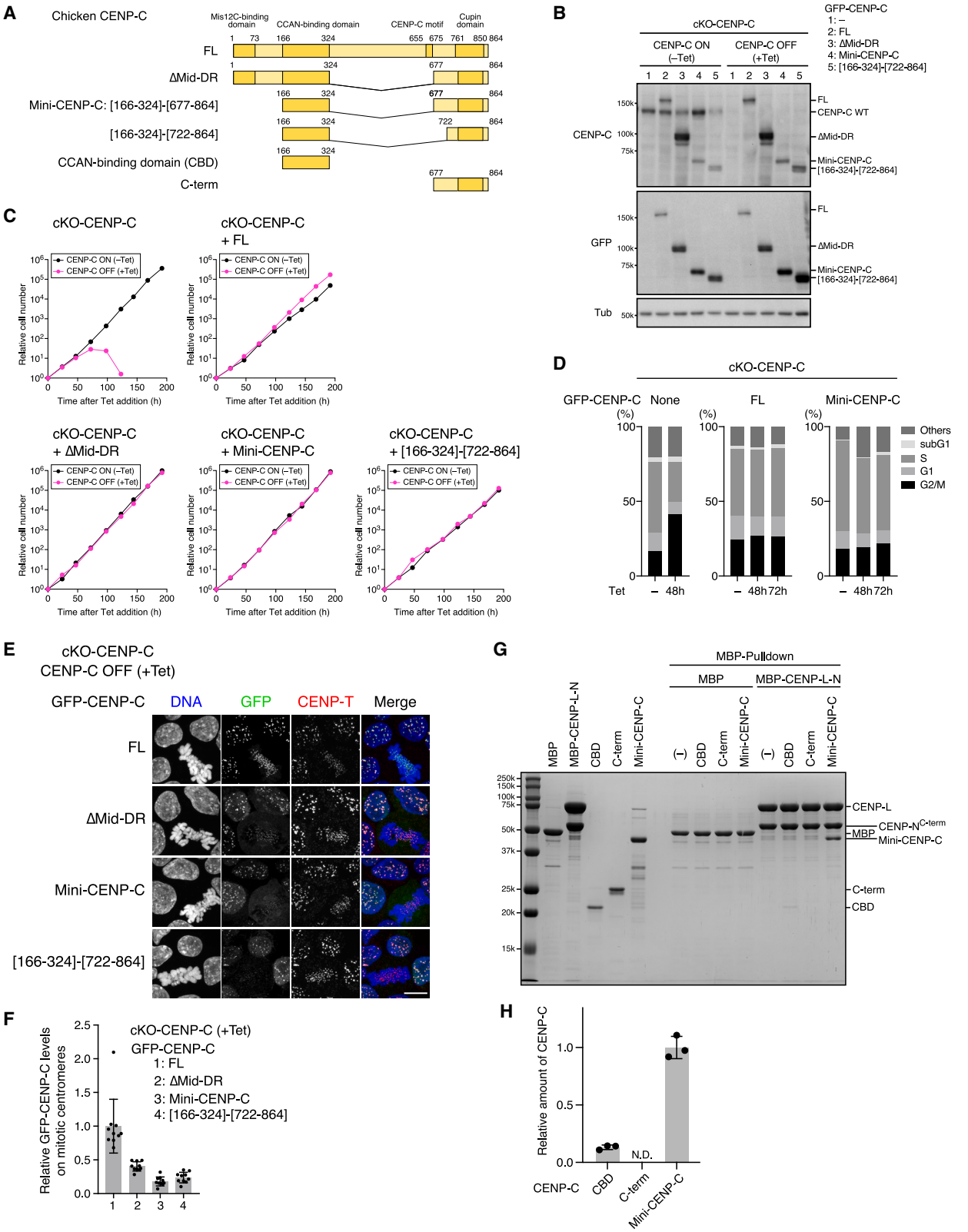

(legend on next page)

GFP-Mini-CENP-C (Figures S1A–S1C). Similar to the CENP-C KO cells expressing GFP-CENP-C^{FL}, CENP-C KO cell lines expressing GFP-Mini-CENP-C were viable and grew (Figure S1D), supporting the sufficiency of Mini-CENP-C for CENP-C function in DT40 cells.

Notably, the CBD and C terminus with the Cupin domain must be fused and expressed as Mini-CENP-C for proper CENP-C function because these domains expressed separately could not suppress the CENP-C deficient phenotype (Figures S1E–S1G). This suggests that the two domains are functionally coupled.

Next, we examined the centromeric localization of Mini-CENP-C. In interphase, Mini-CENP-C as well as CENP-C$^{\Delta Mid\text{-}DR}$ and CENP-C$^{[166–324]\text{-}[722–864]}$ presented centromeric localization in Tet-treated cKO-CENP-C cells (Figure 2E). The signals of these truncated CENP-C diffused somewhat into the interphase nuclei, suggesting a possible contribution of the middle-disordered region to the proper centromeric localization. Nevertheless, this disordered region was dispensable for the CENP-C function (Figures 2C and 2D).

CENP-C localization in interphase centromeres relies on the CENP-H-I-K-M and CENP-L-N subcomplexes.[20,41,42] Although CBD binds to CENP-H-I-K-M and CENP-L-N in vitro,[20,34,37,47] GFP-CENP-C^{CBD} expressed in cKO-CENP-C cells did not localize to the centromeres (Figure S1H). Since Mini-CENP-C localized to centromeres in interphase cells, the CBD should be considered to require the C terminus for centromeric localization (Figure 2E), implying inadequate CBD affinity to CCAN subcomplexes; the C-terminal region, including the Cupin domain, strengthens interactions between the CBD and CCAN subcomplexes for centromere localization in cells. To verify this hypothesis, we examined the binding of CBD to the CENP-L-N complex (MBP-CENP-L/MBP-CENP-N$^{C\text{-}term}$, MBP-CENP-L-N) using an in vitro pull-down assay. CBD scarcely precipitated with CENP-L-N-bound beads. Contrastingly, Mini-CENP-C bound efficiently to the CENP-L-N complex (Figures 2G and 2H). The C terminus with the Cupin domain did not directly bind to the CENP-L-N complex (Figures 2G and 2H), indicating that the C-terminal region leads to the robust binding of the CBD to the CENP-L-N complex. This is because avidity effect of CBD oligomerization through the C-terminal region (see below).

Although Mini-CENP-C as well as CENP-C$^{\Delta Mid\text{-}DR}$ and CENP-C$^{[166–324]\text{-}[722–864]}$ showed noticeable centromeric localization in interphase cells, their centromeric localization was less evident in mitotic cells compared with CENP-C^{FL} (Figures 2E and 2F). This can be attributable to the fact that CENP-C localization to mitotic centromeres is largely dependent on the CENP-A-binding of the CENP-C motif,[36,43] which is absent from the truncated CENP-C mutants (Figure 2A).

Considering that CENP-C facilitates the CENP-A stability at the centromere in human cells,[48] we examined CENP-A localization to centromeres in cKO-CENP-C cells and observed that CENP-A levels at the centromeres were reduced after inhibition of CENP-C expression (Figures S1I and S1J). The CENP-A reduction was rescued by CENP-C^{FL} and Mini-CENP-C (Figures S1I and S1J). This result confirms that Mini-CENP-C is sufficient for CENP-C function in DT40 cells.

Structure of the Cupin domain of chicken CENP-C

CBD directly binds to the CENP-H-I-K-M and CENP L-N subcomplexes.[20,34,37,47] The cryo-electron microscopic analyses have proposed structural models supporting this.[26,27] Consistent with the in vitro studies, the CBD was essential for CENP-C function in cells (Figures 1C and 1D). However, the CBD alone was not sufficient for the centromeric localization and function of CENP-C in cells. Since the CBD requires the C terminus that includes the Cupin domain for the CENP-C function (Figures 2E and S1H), its action mechanism needs to be explored.

Previous structural studies of the Cupin domain of yeast and fly CENP-C homologs revealed that the Cupin domains formed a homodimer.[38–40] Although the vertebrate CENP-C Cupin domain was thought to form a homodimer, it was suggested to form oligomers in human cells.[49] To clarify the molecular characteristics of the vertebrate CENP-C Cupin domain, we determined the crystal structure of the chicken CENP-C$^{C\text{-}term}$ at 2.64 Å resolution (Figure 3A; Table S1). The overall structure of CENP-C$^{C\text{-}term}$ featured a classical Cupin fold consisting of nine β-strands (β5–β13, aa 761–850) with an additional structural region (aa 722–760), which was termed "pre-Cupin" (Figures 3A, 3B, and S2A). The N- and C-terminal regions of the CENP-C$^{C\text{-}term}$, aa 677–721 and aa 851–864, respectively, were disordered. The Cupin fold of chicken CENP-C indeed formed a stable homodimer interface, which appeared similar to its counterpart in other species[38–40] (Figures 3B and S2B). There, K777, Y799, and H843 contributed to dimer interface

Figure 2. CCAN-binding domain and C-terminal region including Cupin domain are sufficient for chicken CENP-C function

(A) Schematic representation of chicken CENP-C mutants. A disordered region (aa 325–676, Mid-DR) predicted by IUPred3[46] was deleted in CENP-C$^{\Delta Mid\text{-}DR}$. The CCAN-binding domain (aa 166–324, CBD) was fused with the C-terminal region, including the Cupin domain, in CENP-C [166–324]-[677–864] (Mini-CENP-C). In CENP-C [166–324]-[722–864] the shorter C-terminal region (aa 722–864) was fused with CBD.

(B) GFP-fused CENP-C expression in cKO-CENP-C DT40 cells. The cells were cultured with or without Tet (+Tet or −Tet) for 48 h.

(C) Growth of cKO-CENP-C cells expressing GFP-CENP-C FL, ΔMid-DR, Mini-CENP-C, or [166–324]-[722–864]. The cell numbers were normalized to those at 0 h for each line.

(D) Cell cycle in cKO-CENP-C cells expressing GFP-CENP-C FL, ΔMid-DR, Mini-CENP-C, or [166–324]-[722–864].

(E and F) GFP-CENP-C FL, ΔMiid-DR, Mini-CENP-C, or [166–324]-[722–864] localization in cKO-CENP-C. The cells were cultured as in (B). Scale bar, 10 μm. GFP-CENP-C signals on centromere in mitotic cells were quantified in (F). (Unpaired t test, two-tailed, mean ± SD, n = 10, FL vs. ΔMid-DR: $p = 0.0002$, FL vs. Mini-CENP-C: $p < 0.0001$, FL vs. [166–324]-[722–864]: $p < 0.0001$).

(G and H) MBP pull-down of CENP-C with MBP-CENP-L-N complex. The CENP-C fragments (CBD, C-term, Mini-CENP-C) were pulled down with MBP-CENP-L-N-complex-bound beads (CENP-L [aa 13–344] and CENP-N C terminus [aa 252–344]) or MBP (MBP-AviTag-His6). The signal intensity of the CENP-C fragment pulled down with MBP-CENP-L-N was quantified and the adjusted values were normalized with the signal intensity of Mini-CENP-C (H). (Unpaired t test, two-tailed, mean ± SD, n = 3, CBD vs. Mini-CENP-C: $p < 0.0001$).

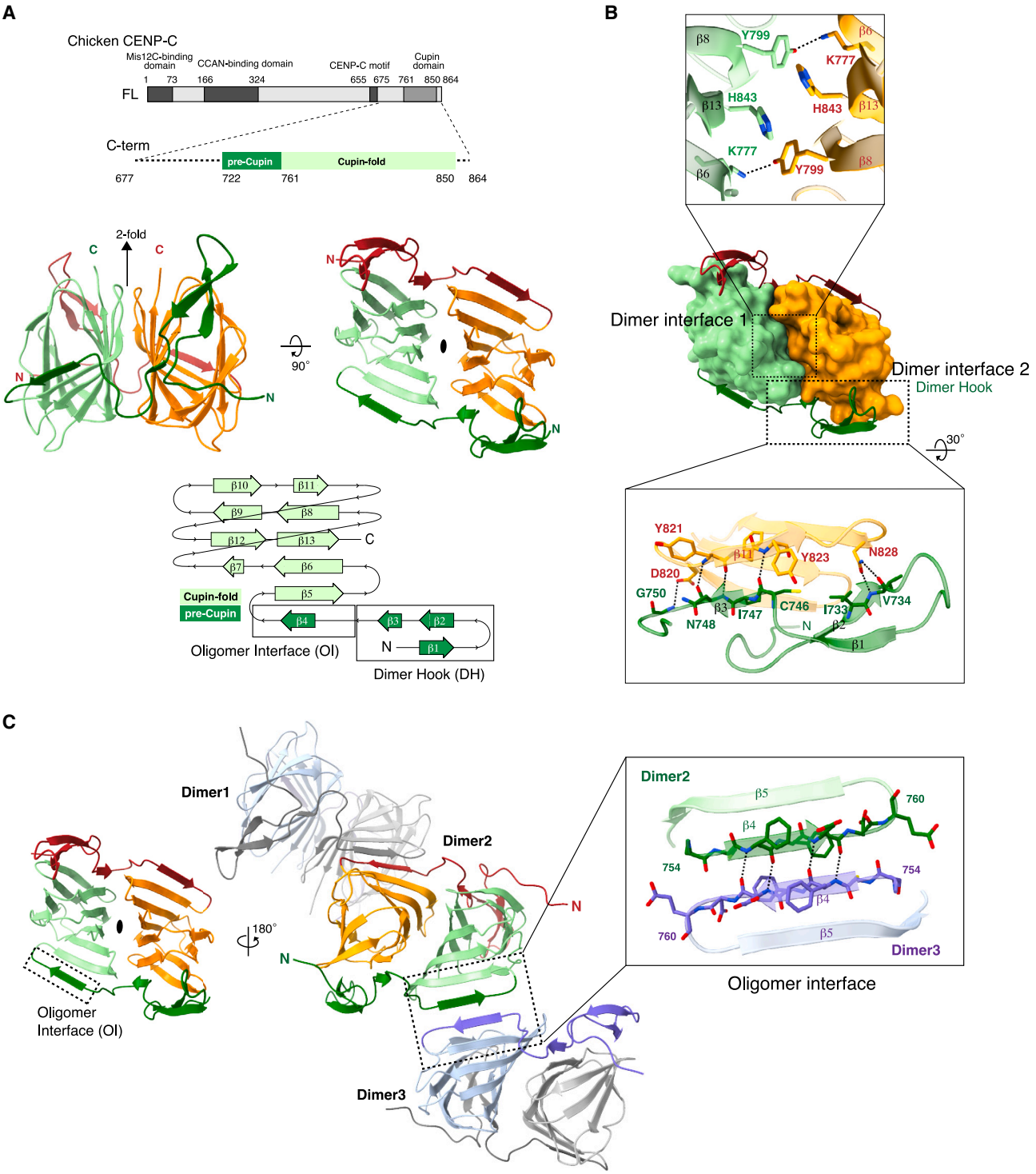

Figure 3. The structure chicken CENP-C$^{C\text{-term}}$

(A) Crystal structure of a dimer of chicken CENP-C$^{C\text{-term}}$ formed by the Cupin domain. A schematic representation of the chicken CENP-C$^{C\text{-term}}$ (aa 677–864) used for structural analysis (top). The Cupin monomers (green and orange) formed a dimeric structure (middle). The pre-Cupin is colored in bright green or dark orange. A secondary structure representation of the chicken Cupin domain (bottom). The pre-Cupin contains the second dimeric interface, dimer hook (DH), and the oligomer interface (OI).

(legend continued on next page)

formation (Figure 3B, Dimer interface 1). Furthermore, the N-terminal part of the pre-Cupin (aa 722–753), termed "dimer hook" (DH), provides an additional dimer interface, absent in *Saccharomyces cerevisiae* CENP-C homolog Mif2p (Figures 3A and 3B, DH, Dimer interface 2). The DH of one subunit was associated with the Cupin fold of another: the β3 strand in one subunit was associated with the β11 strand in another (Figure 3B). The structure suggests that both the classical Cupin fold interface and the DH-mediated interface are involved in chicken CENP-C dimer formation.

To assess the biological significance of the dimer interfaces identified in the crystal structure, we generated mutants focusing on these interfaces in view of inducing disrupted homodimer formation: alanine substitutions in the classical Cupin fold (Y799A/H843A: Cupin_Mut), DH deletion (Δ725-753: ΔDH), or a combination of both (Δ725-753/Y799A/H843A: ΔDH/Cupin_Mut) (Figures 3B and S3A). Each CENP-C mutant was expressed in cKO-CENP-C cells to determine whether CENP-C deficiency was restored (Figure S3B). The growth after Tet addition of cKO-CENP-C cells expressing CENP-C^{Cupin_Mut}, or CENP-$C^{\Delta DH}$, was comparable with that of the cKO-CENP-C cells expressing CENP-C^{FL}, whereas cKO-CENP-C cells expressing CENP-$C^{\Delta DH/Cupin\_Mut}$ exhibited growth retardation (Figure S3C). Previous reports demonstrated the importance of the dimerized Cupin domain in the CENP-C function.[38,39] These results indicate that both the classical Cupin fold and the DH contribute to the CENP-C dimerization, and either one is sufficient for chicken CENP-C dimerization. GFP-fused CENP-C^{Cupin_Mut} and CENP-$C^{\Delta DH}$ localized to centromeres in the Tet-treated cKO-CENP-C cells, but CENP-$C^{\Delta DH/Cupin\_Mut}$ did not, which indicates the importance of dimerization of CENP-C for its localization (Figures S3D and S3E).

Cupin domain of vertebrate CENP-C forms a self-oligomer

In addition to homodimerization of the Cupin domain, the crystal packing analysis of chicken CENP-$C^{C\text{-}term}$ suggested the further self-oligomerization of the Cupin dimers, which was mediated by intermolecular β-sheet formation (Figure 3C). Notably, this putative oligomerization interface comprised the main chain of the β4 strands (aa 755–758) of the pre-Cupin, the unique part of chicken CENP-C, which is conserved among vertebrates (Figure S2A). We termed this region (aa 754–760), including the β4 strands as an oligomer interface (OI) (Figures 3C and S2).

To validate the oligomerization of the CENP-$C^{C\text{-}term}$ in solution, we used blue native polyacrylamide gel electrophoresis (BN-PAGE); chicken CENP-$C^{C\text{-}term}$ showed a ladder of bands, whereas the Mif2p C terminus that includes the Cupin domain (aa 307–549, $Mif2p^{C\text{-}term}$) was observed as a monomer or dimer (Figures 4A and 4B). This outcome further illustrates the formation of chicken Cupin domain oligomers.

To evaluate the role of the β4 strand (OI) in the Cupin domain oligomerization, we substituted residues in the β4 strand with proline to perturb the backbone hydrogen bond interactions between the two β4 strands, as previously reported to prevent IL8 dimer formation.[50] The structural model of the CENP-$C^{C\text{-}term}$ with proline substitutions in F756 and F757 predicted using AlphaFold2 showed a disrupted β4 strand, but the dimer was maintained (Figure 4C). Consistent with the structural prediction, the CENP-$C^{C\text{-}term}$ with F756P and F757P (CENP-$C^{C\text{-}term\ PP}$) exhibited a less clear ladder attributed to self-oligomerization compared with that of the wild-type CENP-$C^{C\text{-}term}$, detected using BN-PAGE analysis (Figures 4D and 4E).

We examined the Cupin domain oligomerization of human CENP-C (hCENP-C) since pre-Cupin appears to be conserved among vertebrate CENP-C proteins (Figure S2A). BN-PAGE revealed a ladder of bands representing hCENP-$C^{C\text{-}term}$ (aa 760–943), including the pre-Cupin and Cupin domain (Figures 4F and 4G, WT). Such ladder formation was prevented by the deletion of a region corresponding to the OI in chicken pre-Cupin from hCENP-$C^{C\text{-}term}$ (Figures 4F and 4G, Δ846-851, ΔOI). These results indicate the oligomerization of the hCENP-C Cupin domain by the β4 strand.

OI is required for the CENP-C function

To examine the physiological significance of the OI (aa 754–760) identified by the structural analyses (Figure 3C), we deleted the OI from chicken CENP-C^{FL} (CENP-$C^{\Delta OI}$) (Figure 5A) and expressed GFP-CENP-$C^{\Delta OI}$ in the cKO-CENP-C cells (Figure 5B). In contrast to CENP-C^{FL} expression, showing rescued growth after Tet treatment, CENP-$C^{\Delta OI}$ expression could not restore the complete growth, suggesting that the OI including the β4 strand in the pre-Cupin is crucial for chicken CENP-C function in DT40 cells (Figure 5C).

The cKO-CENP-C cells expressing CENP-$C^{\Delta OI}$ increased the cell population at the G2/M phase after Tet treatment (Figure 5D), suggesting a mitotic delay in these cells. To further analyze the mitotic defect, we assessed chromosome alignment in the cKO-CENP-C cells expressing CENP-$C^{\Delta OI}$. These cells were treated with MG132 to enrich the mitotic cells. Z-stack images of the centromeres in mitotic cells were obtained using confocal microscopy and projected onto a 2D plane. The resulting scatter plot was analyzed using confidence ellipses (Figure 5E). Chromosomal alignment was evaluated using the ratio of the semi-major axis to the semi-minor axis of the ellipse (Figure 5E, alignment values). Alignment values decreased in cKO-CENP-C cells after Tet treatment, suggesting increased chromosome misalignment (Figure 5E). The chromosome alignment defects were resolved by expressions of CENP-C^{FL} and Mini-CENP-C rather than CENP-$C^{\Delta OI}$. These results indicated that CENP-C requires OI for chromosome alignment and mitotic progression.

(B) Dimeric interfaces of the Cupin dimer. The Cupin dimer is shown in surface model of the Cupin fold and ribbon representation of the pre-Cupin. The insets show the conserved interface (top, Dimer interface1) and the second interface between the dimer Hook in the pre-Cupin and the Cupin fold of another monomer (bottom, Dimer interface 2).

(C) A high-order oligomeric structure of the Cupin dimers found in the crystal packing analyses. The Cupin dimers interact through main chain hydrogen bonds provided by β4 strands (inset).

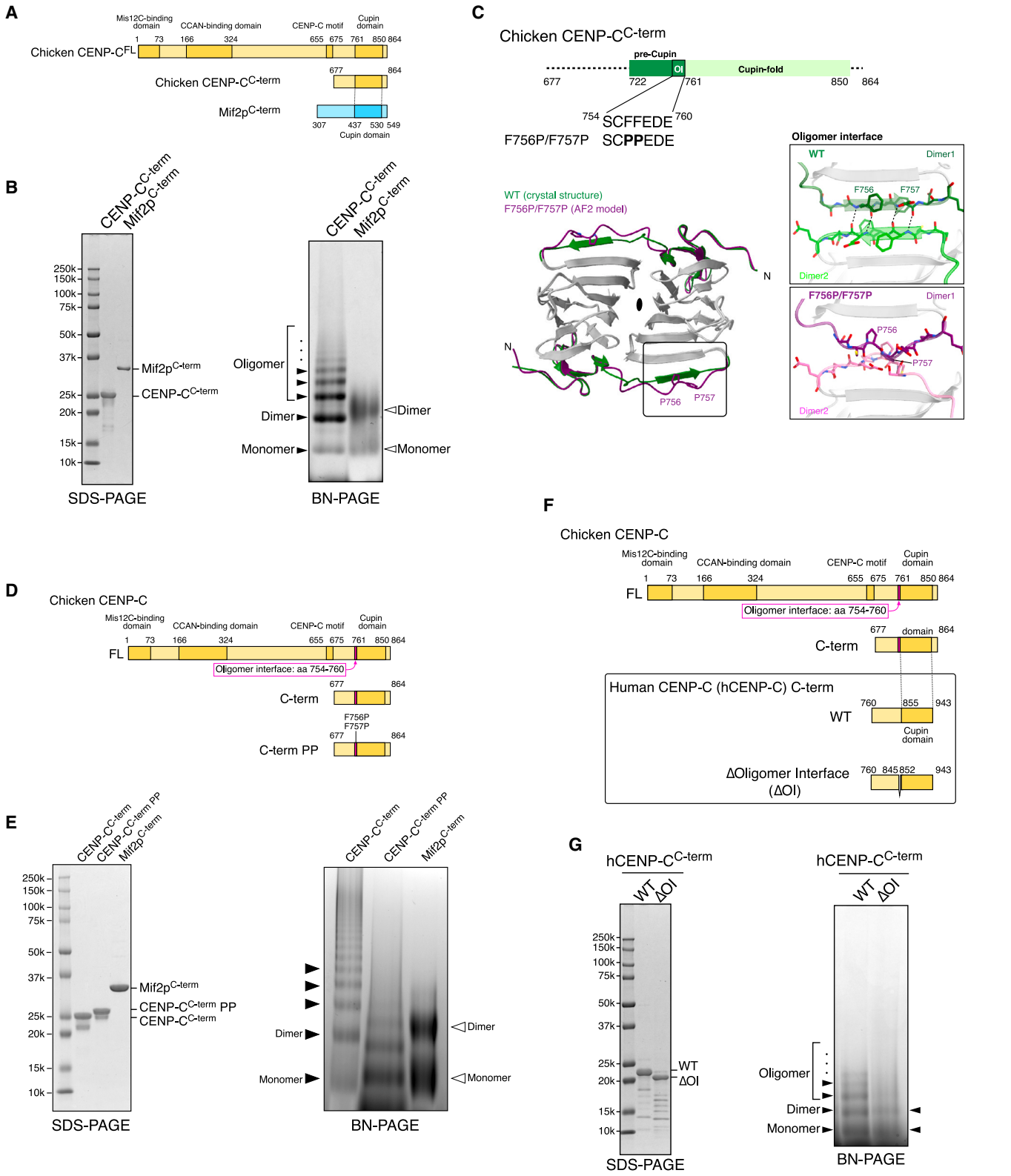

Figure 4. The CENP-C cupin dimer forms higher-order oligomers

(A) Schematic representation of chicken CENP-C$^{C\text{-term}}$ (aa 677–864) and yeast CENP-C homolog Mif2p$^{C\text{-term}}$ (307–549).

(B) Chicken CENP-C$^{C\text{-term}}$ and Mif2p$^{C\text{-term}}$ were examined using SDS-PAGE (left) and Blue Native (BN)-PAGE (right).

(legend continued on next page)

Subsequently, we examined CENP-C$^{\Delta OI}$ localization. Although the protein levels of GFP-CENP-C$^{\Delta OI}$ were comparable with those of the GFP-CENP-C^{FL} in Tet-treated cKO-CENP-C cells (Figures 5B and S3F), the centromeric signals of GFP-CENP-C$^{\Delta OI}$ were not detectable during either interphase or mitosis, whereas GFP-CENP-C^{FL} localized to the centromeres in both phases (Figure 5F). Both the CBD and CENP-C motifs associated with CCAN proteins and the CENP-A nucleosome, respectively, are present in the CENP-C$^{\Delta OI}$ (Figure 5A). These domains appear to be insufficient for the localization of CENP-C to the centromeres (Figure 5F). However, CENP-C localization through these domains requires the OI.

To examine whether OI-dependent centromeric localization of CENP-C is required for the localization of CCAN proteins to centromeres, we quantified the levels of the CENP-N and CENP-T at the mitotic centromeres (Figures 5F and 5G). Their levels at mitotic centromeres were reduced in Tet-treated cKO-CENP-C cells; however, the levels were recovered by GFP-CENP-C^{FL} (Figures 5F and 5G). The GFP-CENP-C$^{\Delta OI}$ expression did not recover both CENP-N and CENP-T levels, suggesting that the OI-dependent CENP-C localization is required for the CCAN protein localization to centromeres (Figures 5F and 5G). Supporting this conclusion, the CENP-N protein reduction at the mitotic centromeres was suppressed by Mini-CENP-C, but neither by CENP-C$^{\Delta CBD}$ nor CENP-C$^{\Delta C\text{-term}}$ (Figure S4). These results suggest that the OI-dependent centromeric localization of CENP-C is crucial for CCAN assembly in DT40 cells.

The proline substitution at F756 and F757 in OI inhibited oligomerization of the chicken CENP-C$^{C\text{-term}}$ in vitro (Figures 4D and 4E). We expressed CENP-C with F756P and F757P substitutions (CENP-C^{PP}) in cKO-CENP-C DT40 cells (Figures 5H and 5I). CENP-C^{PP} did not restore cellular growth and accurate localization in cKO-CENP-C cells after Tet treatment (Figures 5J–5L). These results suggest that CENP-C oligomerization through OI is crucial for its function in chicken DT40 cells.

Moreover, we tested whether OI was essential for hCENP-C function using human RPE1 cells, in which the hCENP-C protein was conditionally depleted by the auxin-inducible degron system (AID)[36] (RPE-1 hCENP-C-AID cells) (Figures S5A and S5B). In RPE-1 hCENP-C-AID cells, indole-3-acetic acid (IAA) led to hCENP-C depletion and defects in cell proliferation (Figures S5B and S5C). The cell proliferation was restored by GFP-hCENP-C^{FL} rather than GFP-hCENP-C$^{\Delta OI}$ (Figures S5A–S5C). OI deletion hampered hCENP-C localization to centromeres (Figures S5D and S5E). Provided OI deletion prevented hCENP-C$^{C\text{-term}}$ oligomer formation in vitro (Figures 4F and 4G), these results suggest that CENP-C oligomerization via OI is also crucial for hCENP-C function in human RPE-1 cells.

Artificial oligomerization of CENP-C facilitates centromeric localization of the CCAN

The above results implied that CENP-C oligomerization was crucial for CENP-C function. To verify this hypothesis, we used an artificially inducible oligomerization system in which an engineered FK506 binding protein (DmrB) that forms homodimer by a small chemical dimerizer (B/B Homodimerizer) is tandemly repeated to allow self-oligomer formation[51,52] (Figures S5F and S5G). Indeed, GFP-fused three tandem repeats of DmrB (3XDmrB), but not single DmrB (1XDmrB), formed condensates in DT40 cells after dimerizer addition (Figure S5G), indicating that 3XDmrB proteins were oligomerized in DT40 cells.

To evaluate the significance of CENP-C oligomerization, we swapped the pre-Cupin and Cupin fold regions of GFP-Mini-CENP-C with either 1XDmrB or 3XDmrB (CENP-C$^{CBD\text{-}1XDmrB}$ or CENP-C$^{CBD\text{-}3XDmrB}$) and expressed either of them or GFP-CENP-C^{CBD} (control) in cKO-CENP-C cells (Figures 6A and 6B). Neither GFP-CENP-C^{CBD} nor GFP-CENP-C$^{CBD\text{-}1XDmrB}$ rescued the growth in Tet-treated cKO-CENP-C with or without the dimerizer (Figure 6C). G2/M enrichment after Tet treatment was observed by GFP-CENP-C$^{CBD\text{-}1XDmrB}$ with or without the dimerizer (Figure 6D). In contrast, in cKO-CENP-C cells expressing GFP-CENP-C$^{CBD\text{-}3XDmrB}$, the dimerizer addition partially but substantially suppressed the growth defect and G2/M enrichment after Tet treatment (Figures 6C and 6D). These results suggest that CBD dimerization is insufficient, but its oligomerization is crucial for CENP-C function in DT40 cells.

Consistent with the suppressed growth defects and G2/M cell enrichment, GFP-CENP-C$^{CBD\text{-}3XDmrB}$ localized to centromeres in the presence of the dimerizer; however, it was not detectable without the dimerizer (Figure 6E). Since GFP-CENP-C$^{CBD\text{-}1XDmrB}$ did not localize to the centromeres after the dimerization step, these results suggest that the oligomerization of CBD is necessary and sufficiently effective for its centromeric localization. Moreover, artificial oligomerization of CBD by 3XDmrB restored CENP-N and CENP-T levels on mitotic centromeres, which were reduced in cKO-CENP-C cells after Tet addition (Figures 6E and 6F). These data strongly propose that CENP-C oligomerization facilitates its kinetochore localization, leading to CCAN assembly.

CENP-C and its OI are involved in the self-association of centromeric chromatin

Centromeric chromatin, which includes CENP-A and H3 nucleosomes with specific histone modifications, is known to have unique three-dimensional structures.[1,53–56] Using 4C-seq analysis of neocentromeres in DT40 cells, we demonstrated previously that centromeric chromatin is self-associated.[57] Since CCAN is directly associated with centromeric chromatin, we

(C) A model of the oligomer interface mutant of chicken Cupin domain predicted by AlphaFold2. F756 and F757 in the oligomer interface were replaced with prolines in the mutant (top). The predicted model of the dimeric F756P/F757P mutant Cupin is overlayed on the crystal structure of the wild-type dimer (left bottom). Zoom in of each oligomer interface is shown (right bottom).
(D) Schematic representation of chicken CENP-C^{FL}, CENP-C$^{C\text{-term}}$, CENP-C$^{C\text{-term PP}}$.
(E) Chicken CENP-C$^{C\text{-term PP}}$ was examined using SDS-PAGE (left) and Blue Native (BN)-PAGE (right) along with wild-type CENP-C$^{C\text{-term}}$ and Mif2p$^{C\text{-term}}$.
(F) Schematic representation of the C-terminal region of human CENP-C (aa 760–943) wild-type (WT) and a mutant, which lacks the region corresponding to the oligomerization interface (ΔOI, Δ846-851).
(G) hCENP-C$^{C\text{-termWT}}$ and hCENP-C$^{C\text{-term }\Delta OI}$ were examined using SDS-PAGE (left) and Blue Native (BN)-PAGE (right).

CellPress
OPEN ACCESS

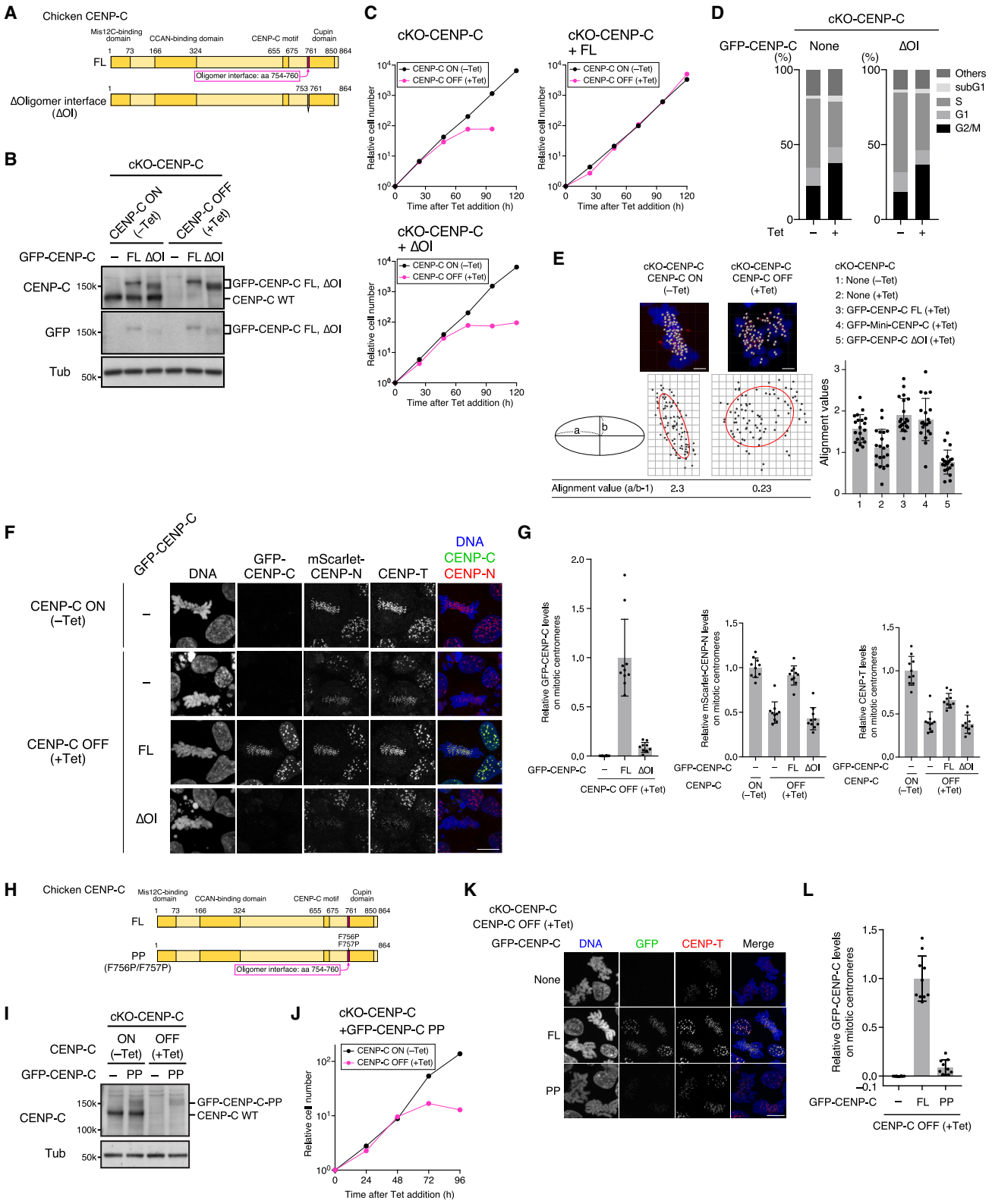

Figure 5. The oligomer interface is required for CENP-C function in chicken DT40 cells

(A) Schematic representation of the chicken CENP-C mutant. The oligomer interface (aa 754–760, OI) was deleted in CENP-C$^{\Delta OI}$.

(B) GFP-fused CENP-C expression in cKO-CENP-C DT40 cells. The cells were cultured with or without Tet (+Tet or −Tet) for 48 h.

(legend continued on next page)

hypothesized that CENP-C and its oligomerization may be involved in centromeric chromatin formation.

We quantitatively verified the self-association within centromeres at the sequence level following a 3C-qPCR method,[58] using the DT40 cell line containing a neocentromere at the 35 Mb region of the Z chromosome[57,59] (neocentromere cell) (Figure S6A). The 3C-qPCR revealed higher ligation frequencies at the 35 Mb region in the neocentromere cells than in the control cells, indicating the efficacy of 3C-qPCR in detecting unique self-associated chromatin characteristics in the neocentromere (Figures S6A and S6B). Thereafter, we examined the involvement of CENP-C in centromeric chromatin organization within the neocentromere, using the AID to deplete the CENP-C protein.[57] AID-tagged CENP-C was rapidly depleted within 2 h of IAA treatment, inducing no change in cell cycle distribution (Figures S6C and S6D). In CENP-C-depleted neocentromere cells (+IAA), the ligation frequencies of all tested sites in the neocentromere were reduced compared with those in untreated cells (–IAA) (Figure S6E). We also observed a reduction in ligation frequency in the neocentromeres of CENP-H-depleted cells[57]; however, the change was smaller than that recorded after CENP-C disruption (Figure S6E). CENP-H depletion increased the G2/M population, but the G2/M-phase enrichment was unlikely attributed to changes in ligation frequencies because the ligation frequencies were largely unaffected by the nocodazole-induced G2/M-phase enrichment (Figures S6F and S6G). These results suggest that CENP-C and CENP-H are involved in self-associated chromatin formation within the neocentromere.

Chicken Chr.Z contains a non-repetitive centromere at the 42 Mb region.[57,59–61] Considering this unique advantageous feature, we investigated whether CENP-C was involved in self-association within the native centromere using 3C-qPCR (Figures 7A and S6H). Ligation frequencies within the native centromere region were reduced in the Tet-treated cKO-CENP-C cells and the reduced values were restored by GFP-CENP-C^{FL} expression (Figures 7B and S6I). CENP-C conditional knockout increased the number of G2/M cells, but the nocodazole-induced G2/M increase did not affect ligation efficiencies (Figures S6I and S6J). These results suggest that CENP-C contributes to the self-association of native centromeric chromatin. To assess CENP-C-dependent centromeric chromatin organization in human RPE-1 cells, we performed super-resolution microscopic analyses of CENP-A distribution in the centromeres. CENP-C depletion led to changes in the CENP-A distribution profile (Figure S7), suggesting that CENP-C is likely involved in the organization of centromeric chromatin in human cells.

Since the CBD and C terminus, including the Cupin domain, are essential for chicken CENP-C function (Figure 1), we examined the involvement of these domains in centromeric chromatin formation using 3C-qPCR. The reduction of ligation frequencies within the centromere in Tet-treated cKO CENP-C cells was not fixed by the expression of CENP-C$^{\Delta CBD}$ or CENP-C$^{\Delta C\text{-term}}$ (Figure S6I). Contrastingly, Mini-CENP-C expression considerably inhibited the reduction in ligation frequency (Figure S6K). Finally, we investigated whether the OI in the pre-Cupin is essential for self-association in centromeric chromatin. Unlike CENP-C^{FL}, CENP-C$^{\Delta OI}$ did not restore the ligation frequencies reduced after Tet addition in cKO-CENP-C cells (Figures 7B and 7C), suggesting that CENP-C oligomerization is required for the CENP-C-dependent self-association of the centromeric chromatin.

DISCUSSION

In this study, we demonstrated the roles of two essential domains in chicken CENP-C function: the CBD and the C-terminal region, which includes the Cupin domain and OI. Mini-CENP-C containing both two was functional, highlighting the functional coupling of the CBD and C-terminal region. Our findings suggest that CBD oligomerization through the C-terminal region is crucial for CENP-C function. The oligomerization facilitated centromeric localization of CENP-C and CCAN assembly on the centromeres, which are required for self-associated centromeric chromatin formation (Figure 7D).

Previous in vitro studies indicated that the CBD of CENP-C binds to the CCAN subcomplexes CENP-H-I-K-M and CENP-L-N.[20,34,37] However, CBD alone was insufficient for stable centromeric localization, indicating inadequate affinity between CBD and the CCAN subcomplexes in cells (Figure 7E). We propose that the CBD oligomerization strengthens the interaction between CENP-C and CCAN at the centromeres as Mini-CENP-C (CBD fused with the C-terminal region, including the OI and Cupin domain) and CBD-3XDmrB (CBD fused with the

(C) Growth of cKO-CENP-C cells expressing GFP-CENP-C FL or ΔOI. The cell numbers were normalized to those at 0 h for each line.
(D) Cell cycle distribution in cKO-CENP-C cells expressing GFP-CENP-C$^{\Delta OI}$.
(E) Chromosome alignment in cKO-CENP-C cells expressing GFP-CENP-C. The distribution of centromeres of mitotic arrested cells by MG132 was projected to a two-dimensional plane and analyzed by using confidence ellipses (red ellipse on the scatter plot: 65% confidence ellipse). Representative images were shown on the left. The alignment values were examined in the indicated cells. Scale bar, 3 μm. (Unpaired t test, two-tailed, mean ± SD, n = 20, None (−Tet) vs. None (+Tet): p = 0.0007, None (+Tet) vs. GFP-CENP-C^{FL} (+Tet): p < 0.0001, None (+Tet) vs. GFP-Mini-CENP-C (+Tet): p < 0.0001, None (+Tet) vs. GFP-CENP-C$^{\Delta OI}$ (+Tet): p = 0.006,).
(F and G) Localization of GFP-CENP-C, mScarlet-CENP-N, and CENP-T in cKO-CENP-C cells. The cells were cultured as in (B). Scale bar, 10 μm. GFP-CENP-C, mScarlet-CENP-N, and CENP-T signals on centromeres in mitotic cells were quantified (G). (Unpaired t test, two-tailed, mean ± SD, GFP, n = 10, −(+Tet) vs. FL (+Tet): p < 0.0001, FL (+Tet) vs. ΔOI (+Tet): p < 0.0001; CENP-N, n = 10, −(−Tet) vs. −(+Tet): p < 0.0001, −(+Tet) vs. FL (+Tet): p < 0.0001, −(+Tet) vs. ΔOI (+Tet): ns (p = 0.2222); CENP-T, n= 10, −(−Tet) vs. −(+Tet): p < 0.0001, −(+Tet) vs. FL (+Tet): p < 0.0001, −(+Tet) vs. ΔOI (+Tet): ns (p = 0.6416)).
(H) Schematic representation of the chicken CENP-C mutant. The residues in the Oligomer interface (F756, F757) were substituted with proline (PP).
(I) GFP-fused CENP-C expression in cKO-CENP-C DT40 cells. The protein expression was examined as in (B).
(J) Growth of cKO-CENP-C cells expressing GFP-CENP-C^{PP}. The cell numbers were examined as in (C).
(K and L) Localization of GFP-CENP-C in cKO-CENP-C cells. The cells were stained as in (F). Scale bar, 10 μm. GFP-CENP-C signals on centromeres in mitotic cells were quantified (L). (Unpaired t test, two-tailed, mean ± SD, n = 10; −(+Tet) vs. FL (+Tet): p < 0.0001, FL (+Tet) vs. PP (+Tet): p < 0.0001).

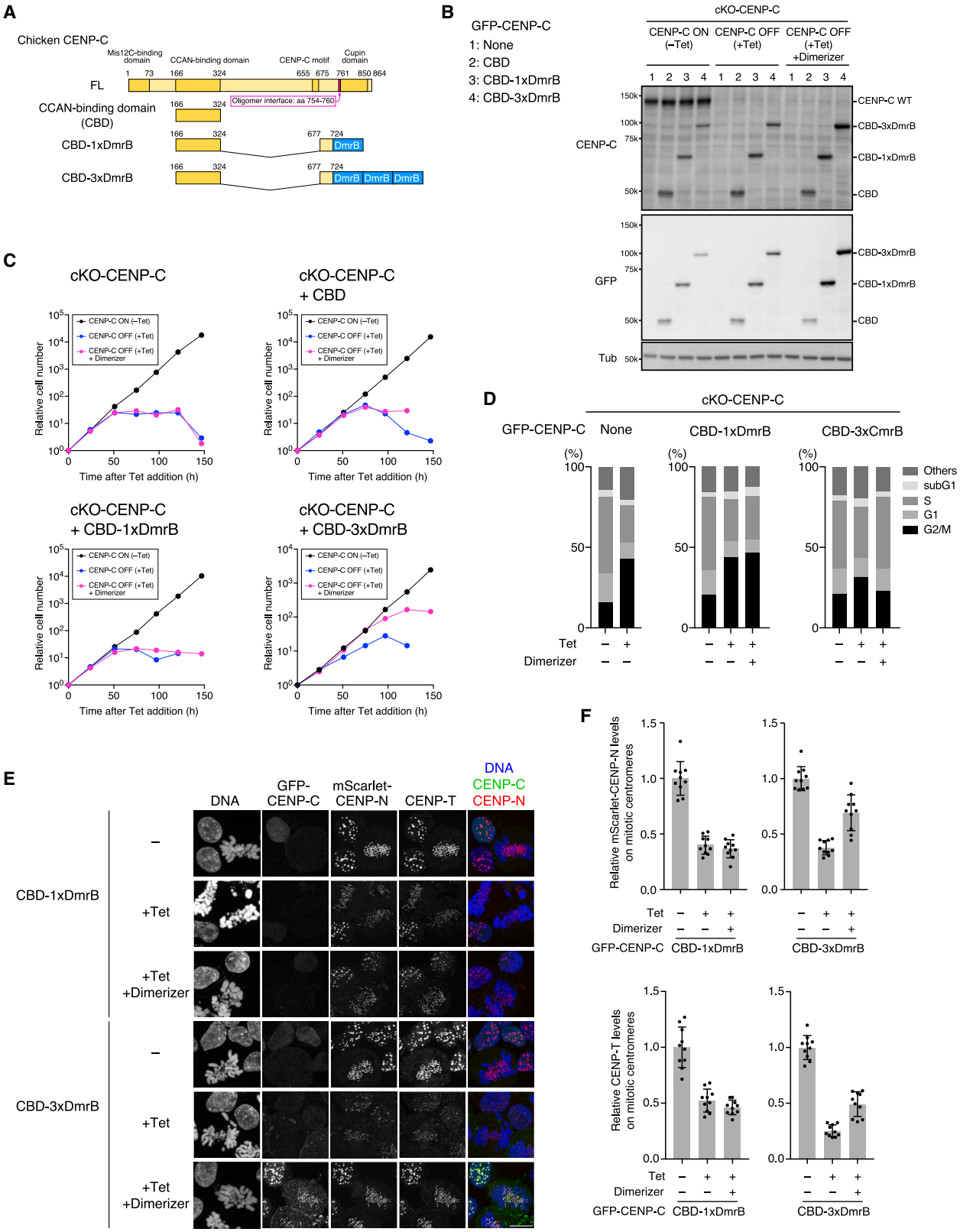

(legend on next page)

artificial oligomerization domain) localized to centromeres. We speculated that the increased local concentration of CENP-C with CCAN at the centromeres facilitates CENP-C oligomerization, which stabilizes CCAN assembly on the centromeres (Figure 7E).

Previously, we reported that the CENP-C motif interacts with the CENP-A nucleosome during mitosis, facilitating centromeric localization of CENP-C.[36] CENP-C$^{\Delta C\text{-term}}$, which includes the CENP-C motif but not the OI, lost its mitotic centromeric localization. Hence, the CENP-C motif-dependent centromeric localization appears to require the oligomerization of Cupin domains.

Homodimerization through the classical Cupin dimer interface is a conserved feature of the Cupin domain of CENP-C in diverse groups of organisms ranging from yeasts to vertebrates.[38–40] Chik et al.[39] demonstrated an additional dimerization interface that strengthens Cupin domain dimerization in *Schizosaccharomyces pombe* and *Drosophila melanogaster* with regional centromeres. However, no additional dimerization interface was detected in CENP-C of *S. cerevisiae* showing point centromeres[39] (Figure S2B). Consistent with this, we identified a DH, an additional dimerization interface in CENP-C of chicken and humans having regional centromeres. Furthermore, an OI that includes a β-strand is associated with the oligomerization of the Cupin dimer in chicken and human CENP-C. Although no equivalent regions of *S. pombe* and *D. melanogaster* were distinctly identified in CENP-C, exploring oligomerization of the CENP-C Cupin domain in invertebrates may reveal noteworthy outcomes.

Recent structural analyses of human CCAN associated with the CENP-A nucleosome have revealed the overall structure of a single CCAN unit and its association with centromeric chromatin.[26,27] However, a large portion of CENP-C, except the PEST-rich domain, was not mapped in these models due to its highly disordered nature.[26,27] Additionally, CENP-C used in the structural analyses lacks a C-terminal region including the Cupin domain.[26,27] Therefore, the current results about the importance of CENP-C oligomerization via the OI and Cupin domain complement those of previous structural studies and imply that CENP-C oligomerization may gather CCAN units, presumably linked with CENP-A nucleosomes, for their stable association with centromeric chromatin. Thus, the results provide deep knowledge about the mechanisms of CCAN assembly on centromeric chromatin.

CCAN must recognize CENP-A nucleosomes to specifically localize to centromeres. Human CENP-C contains two CENP-A-binding regions: the central domain and the CENP-C motif.[62] Deletion of both regions leads to the defective human CENP-C,[36] suggesting its crucial role in recognizing CENP-A nucleosomes. Contrastingly, chicken CENP-C contains one CENP-A-binding domain, the CENP-C motif, which is dispensable for CENP-C function in DT40 cells.[36] Furthermore, this study revealed that Mini-CENP-C, with no CENP-C motif, was functional. These results seek to answer the manner in which the chicken CCAN recognizes CENP-A chromatin. CCAN protein CENP-N binds to CENP-A in vitro[43,47,63–65] and possibly interacts with CENP-A nucleosomes in vivo. However, recent structural studies of human CCAN have found no interaction between CENP-N and the CENP-A nucleosome in the CCAN complex.[26,27] Alternatively, the kinetochore protein KNL2 may target CCAN to the CENP-A nucleosome in chicken cells. KNL2, a part of the Mis18 complex, is required for CENP-A deposition into the centromeric chromatin.[66–70] Notably, the chicken KNL2 includes a CENP-C-motif-like sequence (CENP-C-like motif). The CENP-C-like motif is also found in KNL2 of Xenopus, fish, and plants.[69–72] This motif directly binds to the CENP-A nucleosome.[73] Moreover, KNL2 interacts with CCAN proteins, including CENP-C.[68,74–76] Therefore, KNL2 possibly compensates for the loss of the CENP-C motif (for example, in Mini-CENP-C) to target CCAN to the CENP-A nucleosome in chicken cells. Notably, mammalian KNL2s, including humans, do not have a CENP-C-like motif, which may explain the difference in the importance of CENP-A recognition for CENP-C function.

Unexpectedly, Mini-CENP-C, associated with less clear mitotic centromere localization, rescued CENP-C-deficient phenotypes; it is possibly attributable to the residual Mini-CENP-C that may be sufficient for CENP-C functions during mitosis. Alternatively, Mini-CENP-C possibly functions in interphase for CCAN recruitment and centromeric chromatin establishment. During mitosis, the established centromeres are maintained by remaining CCAN proteins or other factors or both.

Limitations of the study

The central proposal of this study is about the pre-Cupin providing oligomerization beyond a dimer to build the kinetochore. Since Mini-CENP-C is functional without an apparent centromeric localization during mitosis, we speculate a role of the oligomerization in interphase prior to mitosis, but the study does not test this idea.

We used 3xDmrB, an inducible artificial oligomerization domain, to demonstrate the role of Cupin domain oligomerization in the CENP-C function. The constitutively induced 3xDmrB-based oligomers generated different higher-order structures from those assembled by the pre-Cupin and Cupin

Figure 6. Artificial oligomerization of CBD supports its centromere localization and CCAN assembly

(A) Schematic representation of the chicken CENP-C mutant. The CCAN-binding domain (aa 166–324, CBD) was fused with the CENP-C C terminus in which the oligomerization domain was replaced with a single DmrB domain (CBD-1xDmrB) or three tandem-repeated DmrB (CBD-3xDmrB).

(B) GFP-fused CENP-C expression in cKO-CENP-C DT40 cells. The cells were treated with no chemical (−Tet), Tet (+Tet), or both Tet and B/B Homodimerizer (+Tet, +Dimerizer) for 48 h.

(C) Growth of cKO-CENP-C cells expressing GFP-fused CENP-C CBD, CBD-1xDmrB, or CBD-3xDmrB. The cell numbers were normalized to those at 0 h for each line.

(D) Cell cycle distribution in cKO-CENP-C cells expressing GFP-fused CENP-C CBD, CBD-1xDmrB, or CBD-3xDmrB.

(E and F) GFP-CENP-C, mScarlet-CENP-N, and CENP-T localization in cKO-CENP-C cells expressing GFP-CENP-C CBD, CBD-1xDmrB, or CBD-3xDmrB. The cells were cultured as in (B). Scale bar, 10 μm. mScarlet-CENP-N and CENP-T signals on centromeres in mitotic cells were quantified (F). (Unpaired t test, two-tailed, mean ± SD, CENP-N, n = 10, 1xDmrB +Tet/−Dimerizer vs. +Tet/+Dimerizer: ns ($p = 0.381$), 3xDmrB +Tet/−Dimerizer vs. +Tet/+Dimerizer: $p < 0.0001$; CENP-T, n = 10, 1xDmrB +Tet/−Dimerizer vs. +Tet/+Dimerizer: ns ($p = 0.1233$), 3xDmrB +Tet/−Dimerizer vs. +Tet/+Dimerizer: $p < 0.0001$.).

CellPress
OPEN ACCESS

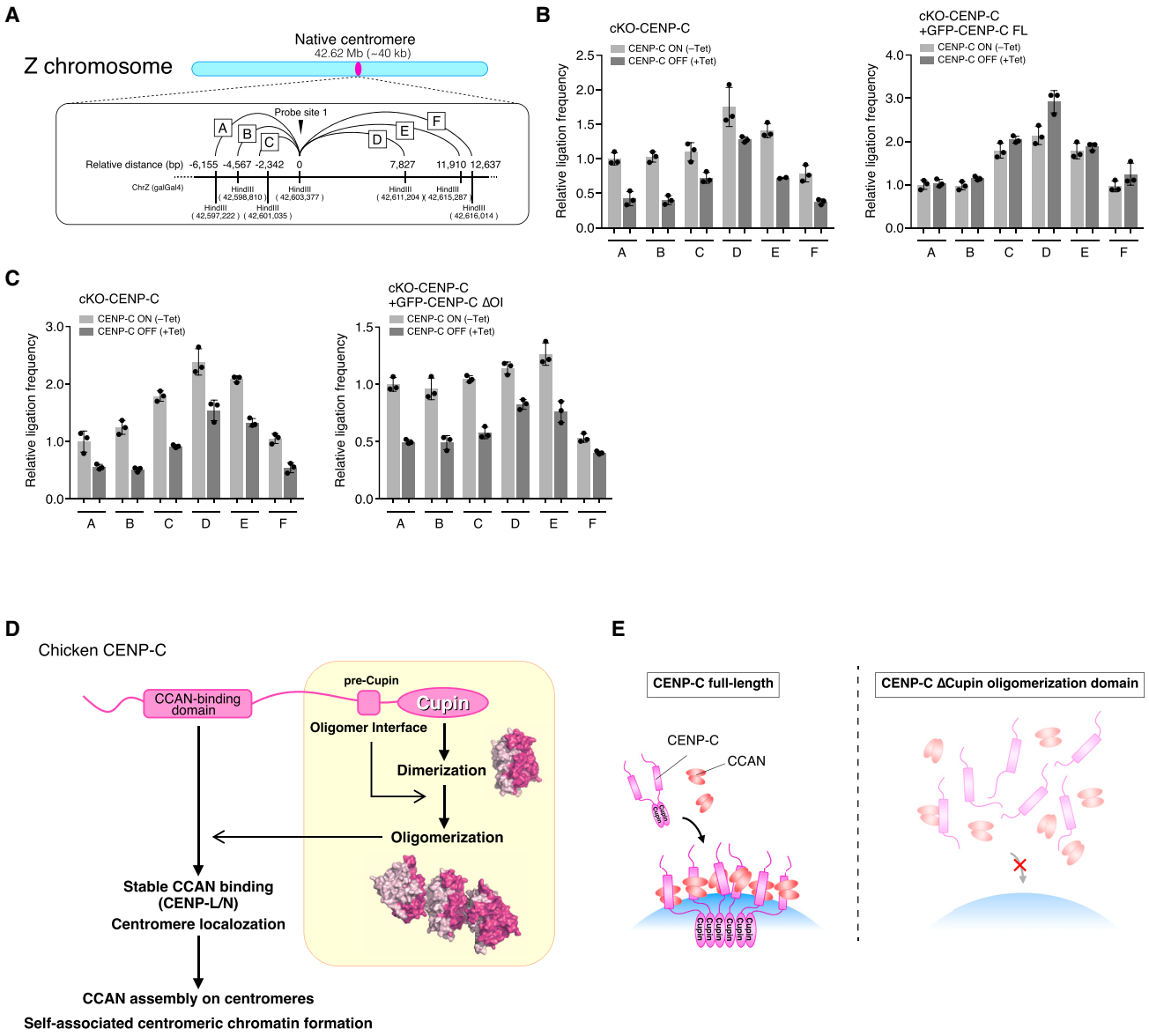

Figure 7. The CENP-C oligomer interface is required for centromeric chromatin formation in DT40 cells

(A) Schematic representation of the chicken Z chromosome. The chicken Z chromosome has a native centromere spanning 40 kb in the 42.6 Mb region.[57,61] The bottom inset shows the 3C-qPCR primer and TaqMan probe positions in the native centromere of the Z chromosome. The TaqMan probe is designed at 5′ (left side) of the HindIII at 0 bp (relative distance, probe site 1). The primers are designed at 5′ of indicated HindIII sites.

(B) 3C-qPCR analysis of centromere chromatin in cKO-CENP-C cells. cKO-CENP-C cells with or without GFP-CENP-C^{FL} expression were fixed at 48 h after treatment with or without Tet. The ligation frequency at the indicated sites within the centromere region was examined and normalized to ligation frequency at site A (−Tet). Error bars, mean ± SD.

(C) 3C-qPCR analysis of centromere chromatin in cKO-CENP-C cells expressing GFP-CENP-C$^{\Delta OI}$. The ligation frequency at the indicated sites in cKO-CENP-C cells expressing GFP-CENP-C$^{\Delta OI}$ was examined as in (B). Error bars, mean ± SD.

(D) The essential domains for chicken CENP-C function. Two conserved domains are crucial for chicken CENP-C function: the CCAN-binding domain and the C-terminal region including the pre-Cupin and Cupin domain. The Cupin domain dimers are oligomerized through the Oligomer interface in pre-Cupin. The oligomerization stabilizes CBD-CCAN binding, which leads to CCAN assembly on centromeres and formation of the centromere specific chromatin.

(E) A model of how CENP-C functions on centromeres. CENP-C is recruited onto centromeres through its CCAN-binding domain. The locally enriched CENP-C proteins on centromeres can be oligomerized and in consequence, stably binds to CCAN proteins. This induces the robust centromeric localization of CCAN including CENP-C, leading to functional kinetochore assembly and self-associated centromeric chromatin organization. Without the oligomerization domain, CENP-C centromeric localization and CCAN-CENP-C interaction were compromised, resulting in the failure of CCAN localization to centromeres and centromeric chromatin organization.

domains of CENP-C. Hence, we could not assess the importance of the higher-order structures of CENP-C oligomers and the dynamic aspects of CENP-C oligomers during cell cycle progression.

The Cupin domain interacts with several kinetochore regulators,[39,40,68,77,78] which was not analyzed in this study. Evaluating the correlation between these interactions and the Cupin domain function can further clarify the role of CENP-C.

We demonstrated that the OI is required for the self-associated centromeric chromatin formation using CENP-C$^{\Delta OI}$. However, since OI deletion prevented CENP-C localization to the centromeres, we could not investigate whether CENP-C oligomerization was directly involved in centromeric chromatin organization.

STAR★METHODS

Detailed methods are provided in the online version of this paper and include the following:

- KEY RESOURCES TABLE
- RESOURCE AVAILABILITY
  - Lead contact
  - Materials availability
  - Data and code availability
- EXPERIMENTAL MODEL AND SUBJECT DETAILS
  - Chicken DT40 cells
  - Human RPE-1 cells
- METHOD DETAILS
  - Cell counting
  - Plasmid constructions
  - Immunoblotting
  - Immunofluorescence
  - Spinning-disk confocal microscopy
  - Quantification of fluorescence signals on mitotic centromeres
  - Chromosome alignment assay
  - Flow cytometry analysis
  - Protein expression and purification
  - Crystallization and structural determination
  - Blue native-polyacrylamide gel electrophoresis (PAGE)
  - In vitro pulldown assay
  - 2D-STORM
  - MINFLUX nanoscopy
  - Rendering 2D-STORM and MINFLUX images
  - Pair correlation analysis
  - 3C-qPCR
- QUANTIFICATION AND STATISTICAL ANALYSIS

SUPPLEMENTAL INFORMATION

Supplemental information can be found online at https://doi.org/10.1016/j.molcel.2023.05.023.

ACKNOWLEDGMENTS

The authors are very grateful to members of the Fukagawa Lab for the fruitful discussion. We also thank R. Fukuoka and K. Oshimo for technical assistance, E. Kakizono and J. Miao for preliminary analyses on this study, J. Cao for sharing plasmids, J. Sha for helping protein purification, D. Fachinetti for providing reagents, and Nikon Solutions Co. Ltd., especially K. Tokunaga for helping STORM imaging. This work was supported by CREST of JST (JPMJCR21E6), JSPS KAKENHI Grant Numbers 17H06167, 20H05389, 21H05752, 22H00408, and 22H04692 to T.F., JSPS KAKENHI Grant Numbers 16K18491 and 21H02461, and Takeda Science Foundation to M.H.

AUTHOR CONTRIBUTIONS

M.H. designed and performed entire experiments in this study. M.A. and T.S. performed structure studies on CENP-C oligomer. R.-S.N., S.S., S.O., I.J., and T.H. performed imaging analyses with SMLM. T.F. contributed to the generation of various DT40 and RPE-1 cell lines. T.F. and M.H. wrote the manuscript, discussing it with all authors.

DECLARATION OF INTERESTS

I.J. is an employee of Abberior Instruments, which develops and manufactures super-resolution fluorescence microscopes, including the MINFLUX system used here. All other authors declare no competing interests.

Received: August 8, 2022
Revised: April 4, 2023
Accepted: May 16, 2023
Published: June 8, 2023

REFERENCES

1. Fukagawa, T., and Earnshaw, W.C. (2014). The centromere: chromatin foundation for the kinetochore machinery. Dev. Cell *30*, 496–508. https://doi.org/10.1016/j.devcel.2014.08.016.
2. McKinley, K.L., and Cheeseman, I.M. (2016). The molecular basis for centromere identity and function. Nat. Rev. Mol. Cell Biol. *17*, 16–29. https://doi.org/10.1038/nrm.2015.5.
3. Hara, M., and Fukagawa, T. (2017). Critical foundation of the kinetochore: the constitutive centromere-associated network (CCAN). Prog. Mol. Subcell. Biol. *56*, 29–57. https://doi.org/10.1007/978-3-319-58592-5_2.
4. Hara, M., and Fukagawa, T. (2018). Kinetochore assembly and disassembly during mitotic entry and exit. Curr. Opin. Cell Biol. *52*, 73–81. https://doi.org/10.1016/j.ceb.2018.02.005.
5. Mellone, B.G., and Fachinetti, D. (2021). Diverse mechanisms of centromere specification. Curr. Biol. *31,* R1491–R1504. https://doi.org/10.1016/j.cub.2021.09.083.
6. Palmer, D.K., O'Day, K., Wener, M.H., Andrews, B.S., and Margolis, R.L. (1987). A 17-kD centromere protein (CENP-A) copurifies with nucleosome core particles and with histones. J. Cell Biol. *104*, 805–815.
7. Okada, M., Cheeseman, I.M., Hori, T., Okawa, K., McLeod, I.X., Yates, J.R., 3rd, Desai, A., and Fukagawa, T. (2006). The CENP-H-I complex is required for the efficient incorporation of newly synthesized CENP-A into centromeres. Nat. Cell Biol. *8*, 446–457. https://doi.org/10.1038/ncb1396.
8. Foltz, D.R., Jansen, L.E., Black, B.E., Bailey, A.O., Yates, J.R., 3rd, and Cleveland, D.W. (2006). The human CENP-A centromeric nucleosome-associated complex. Nat. Cell Biol. *8*, 458–469. https://doi.org/10.1038/ncb1397.
9. Izuta, H., Ikeno, M., Suzuki, N., Tomonaga, T., Nozaki, N., Obuse, C., Kisu, Y., Goshima, N., Nomura, F., Nomura, N., et al. (2006). Comprehensive analysis of the ICEN (Interphase Centromere Complex) components enriched in the CENP-A chromatin of human cells. Genes Cells *11*, 673–684. https://doi.org/10.1111/j.1365-2443.2006.00969.x.
10. Hori, T., Amano, M., Suzuki, A., Backer, C.B., Welburn, J.P., Dong, Y., McEwen, B.F., Shang, W.H., Suzuki, E., Okawa, K., et al. (2008). CCAN makes multiple contacts with centromeric DNA to provide distinct pathways to the outer kinetochore. Cell *135*, 1039–1052. https://doi.org/10.1016/j.cell.2008.10.019.

11. Amano, M., Suzuki, A., Hori, T., Backer, C., Okawa, K., Cheeseman, I.M., and Fukagawa, T. (2009). The CENP-S complex is essential for the stable assembly of outer kinetochore structure. J. Cell Biol. *186*, 173–182. https://doi.org/10.1083/jcb.200903100.

12. Black, B.E., and Cleveland, D.W. (2011). Epigenetic centromere propagation and the nature of CENP-a nucleosomes. Cell *144*, 471–479. https://doi.org/10.1016/j.cell.2011.02.002.

13. Nishino, T., Takeuchi, K., Gascoigne, K.E., Suzuki, A., Hori, T., Oyama, T., Morikawa, K., Cheeseman, I.M., and Fukagawa, T. (2012). CENP-T-W-S-X forms a unique centromeric chromatin structure with a histone-like fold. Cell *148*, 487–501. https://doi.org/10.1016/j.cell.2011.11.061.

14. Westhorpe, F.G., and Straight, A.F. (2013). Functions of the centromere and kinetochore in chromosome segregation. Curr. Opin. Cell Biol. *25*, 334–340. https://doi.org/10.1016/j.ceb.2013.02.001.

15. Cheeseman, I.M., Chappie, J.S., Wilson-Kubalek, E.M., and Desai, A. (2006). The conserved KMN network constitutes the core microtubule-binding site of the kinetochore. Cell *127*, 983–997. https://doi.org/10.1016/j.cell.2006.09.039.

16. DeLuca, J.G., Gall, W.E., Ciferri, C., Cimini, D., Musacchio, A., and Salmon, E.D. (2006). Kinetochore microtubule dynamics and attachment stability are regulated by Hec1. Cell *127*, 969–982. https://doi.org/10.1016/j.cell.2006.09.047.

17. Alushin, G.M., Ramey, V.H., Pasqualato, S., Ball, D.A., Grigorieff, N., Musacchio, A., and Nogales, E. (2010). The Ndc80 kinetochore complex forms oligomeric arrays along microtubules. Nature *467*, 805–810. https://doi.org/10.1038/nature09423.

18. Pesenti, M.E., Weir, J.R., and Musacchio, A. (2016). Progress in the structural and functional characterization of kinetochores. Curr. Opin. Struct. Biol. *37*, 152–163. https://doi.org/10.1016/j.sbi.2016.03.003.

19. Nagpal, H., and Fukagawa, T. (2016). Kinetochore assembly and function through the cell cycle. Chromosoma *125*, 645–659. https://doi.org/10.1007/s00412-016-0608-3.

20. McKinley, K.L., Sekulic, N., Guo, L.Y., Tsinman, T., Black, B.E., and Cheeseman, I.M. (2015). The CENP-L-N complex forms a critical node in an integrated meshwork of interactions at the centromere-kinetochore interface. Mol. Cell *60*, 886–898. https://doi.org/10.1016/j.molcel.2015.10.027.

21. Weir, J.R., Faesen, A.C., Klare, K., Petrovic, A., Basilico, F., Fischböck, J., Pentakota, S., Keller, J., Pesenti, M.E., Pan, D., et al. (2016). Insights from biochemical reconstitution into the architecture of human kinetochores. Nature *537*, 249–253. https://doi.org/10.1038/nature19333.

22. Pesenti, M.E., Prumbaum, D., Auckland, P., Smith, C.M., Faesen, A.C., Petrovic, A., Erent, M., Maffini, S., Pentakota, S., Weir, J.R., et al. (2018). Reconstitution of a 26-subunit human kinetochore reveals cooperative microtubule binding by CENP-OPQUR and NDC80. Mol. Cell *71*, 923–939.e10. https://doi.org/10.1016/j.molcel.2018.07.038.

23. Walstein, K., Petrovic, A., Pan, D., Hagemeier, B., Vogt, D., Vetter, I.R., and Musacchio, A. (2021). Assembly principles and stoichiometry of a complete human kinetochore module. Sci. Adv. *7,* eabg1037. https://doi.org/10.1126/sciadv.abg1037.

24. Yan, K., Yang, J., Zhang, Z., McLaughlin, S.H., Chang, L., Fasci, D., Ehrenhofer-Murray, A.E., Heck, A.J.R., and Barford, D. (2019). Structure of the inner kinetochore CCAN complex assembled onto a centromeric nucleosome. Nature *574*, 278–282. https://doi.org/10.1038/s41586-019-1609-1.

25. Hinshaw, S.M., and Harrison, S.C. (2019). The structure of the Ctf19c/CCAN from budding yeast. Elife *8,* e44239. https://doi.org/10.7554/eLife.44239.

26. Yatskevich, S., Muir, K.W., Bellini, D., Zhang, Z., Yang, J., Tischer, T., Predin, M., Dendooven, T., McLaughlin, S.H., and Barford, D. (2022). Structure of the human inner kinetochore bound to a centromeric CENP-A nucleosome. Science *376*, 844–852. https://doi.org/10.1126/science.abn3810.

27. Pesenti, M.E., Raisch, T., Conti, D., Walstein, K., Hoffmann, I., Vogt, D., Prumbaum, D., Vetter, I.R., Raunser, S., and Musacchio, A. (2022). Structure of the human inner kinetochore CCAN complex and its significance for human centromere organization. Mol. Cell *82*, 2113–2131.e8. https://doi.org/10.1016/j.molcel.2022.04.027.

28. Earnshaw, W.C., and Rothfield, N. (1985). Identification of a family of human centromere proteins using autoimmune sera from patients with scleroderma. Chromosoma *91*, 313–321.

29. Tomkiel, J., Cooke, C.A., Saitoh, H., Bernat, R.L., and Earnshaw, W.C. (1994). CENP-C is required for maintaining proper kinetochore size and for a timely transition to anaphase. J. Cell Biol. *125*, 531–545.

30. Meluh, P.B., and Koshland, D. (1995). Evidence that the MIF2 gene of Saccharomyces cerevisiae encodes a centromere protein with homology to the mammalian centromere protein CENP-C. Mol. Biol. Cell *6*, 793–807.

31. Fukagawa, T., and Brown, W.R. (1997). Efficient conditional mutation of the vertebrate CENP-C gene. Hum. Mol. Genet. *6*, 2301–2308.

32. Kalitsis, P., Fowler, K.J., Earle, E., Hill, J., and Choo, K.H. (1998). Targeted disruption of mouse centromere protein C gene leads to mitotic disarray and early embryo death. Proc. Natl. Acad. Sci. USA *95*, 1136–1141.

33. Fukagawa, T., Pendon, C., Morris, J., and Brown, W. (1999). CENP-C is necessary but not sufficient to induce formation of a functional centromere. EMBO J. *18*, 4196–4209. https://doi.org/10.1093/emboj/18.15.4196.

34. Klare, K., Weir, J.R., Basilico, F., Zimniak, T., Massimiliano, L., Ludwigs, N., Herzog, F., and Musacchio, A. (2015). CENP-C is a blueprint for constitutive centromere-associated network assembly within human kinetochores. J. Cell Biol. *210*, 11–22. https://doi.org/10.1083/jcb.201412028.

35. Hara, M., Ariyoshi, M., Okumura, E.I., Hori, T., and Fukagawa, T. (2018). Multiple phosphorylations control recruitment of the KMN network onto kinetochores. Nat. Cell Biol. *20*, 1378–1388. https://doi.org/10.1038/s41556-018-0230-0.

36. Watanabe, R., Hara, M., Okumura, E.I., Hervé, S., Fachinetti, D., Ariyoshi, M., and Fukagawa, T. (2019). CDK1-mediated CENP-C phosphorylation modulates CENP-A binding and mitotic kinetochore localization. J. Cell Biol. *218*, 4042–4062. https://doi.org/10.1083/jcb.201907006.

37. Nagpal, H., Hori, T., Furukawa, A., Sugase, K., Osakabe, A., Kurumizaka, H., and Fukagawa, T. (2015). Dynamic changes in CCAN organization through CENP-C during cell-cycle progression. Mol. Biol. Cell *26*, 3768–3776. https://doi.org/10.1091/mbc.E15-07-0531.

38. Cohen, R.L., Espelin, C.W., De Wulf, P., Sorger, P.K., Harrison, S.C., and Simons, K.T. (2008). Structural and functional dissection of Mif2p, a conserved DNA-binding kinetochore protein. Mol. Biol. Cell *19*, 4480–4491. https://doi.org/10.1091/mbc.E08-03-0297.

39. Chik, J.K., Moiseeva, V., Goel, P.K., Meinen, B.A., Koldewey, P., An, S., Mellone, B.G., Subramanian, L., and Cho, U.S. (2019). Structures of CENP-C cupin domains at regional centromeres reveal unique patterns of dimerization and recruitment functions for the inner pocket. J. Biol. Chem. *294*, 14119–14134. https://doi.org/10.1074/jbc.RA119.008464.

40. Medina-Pritchard, B., Lazou, V., Zou, J., Byron, O., Abad, M.A., Rappsilber, J., Heun, P., and Jeyaprakash, A.A. (2020). Structural basis for centromere maintenance by Drosophila CENP-A chaperone CAL1. EMBO J. *39,* e103234. https://doi.org/10.15252/embj.2019103234.

41. Kwon, M.S., Hori, T., Okada, M., and Fukagawa, T. (2007). CENP-C is involved in chromosome segregation, mitotic checkpoint function, and kinetochore assembly. Mol. Biol. Cell *18*, 2155–2168. https://doi.org/10.1091/mbc.E07-01-0045.

42. Fukagawa, T., Mikami, Y., Nishihashi, A., Regnier, V., Haraguchi, T., Hiraoka, Y., Sugata, N., Todokoro, K., Brown, W., and Ikemura, T. (2001). CENP-H, a constitutive centromere component, is required for centromere targeting of CENP-C in vertebrate cells. EMBO J. *20*, 4603–4617. https://doi.org/10.1093/emboj/20.16.4603.

43. Ariyoshi, M., Makino, F., Watanabe, R., Nakagawa, R., Kato, T., Namba, K., Arimura, Y., Fujita, R., Kurumizaka, H., Okumura, E.I., et al. (2021). Cryo-EM structure of the CENP-A nucleosome in complex with

phosphorylated CENP-C. EMBO J. *40,* e105671. https://doi.org/10.15252/embj.2020105671.

44. Suzuki, A., Hori, T., Nishino, T., Usukura, J., Miyagi, A., Morikawa, K., and Fukagawa, T. (2011). Spindle microtubules generate tension-dependent changes in the distribution of inner kinetochore proteins. J. Cell Biol. *193*, 125–140. https://doi.org/10.1083/jcb.201012050.

45. Suzuki, A., Badger, B.L., Wan, X., DeLuca, J.G., and Salmon, E.D. (2014). The architecture of CCAN proteins creates a structural integrity to resist spindle forces and achieve proper Intrakinetochore stretch. Dev. Cell *30*, 717–730. https://doi.org/10.1016/j.devcel.2014.08.003.

46. Erdős, G., Pajkos, M., and Dosztányi, Z. (2021). IUPred3: prediction of protein disorder enhanced with unambiguous experimental annotation and visualization of evolutionary conservation. Nucleic Acids Res. *49*. W297–W303. https://doi.org/10.1093/nar/gkab408.

47. Pentakota, S., Zhou, K., Smith, C., Maffini, S., Petrovic, A., Morgan, G.P., Weir, J.R., Vetter, I.R., Musacchio, A., and Luger, K. (2017). Decoding the centromeric nucleosome through CENP-N. Elife *6,* e33442. https://doi.org/10.7554/eLife.33442.

48. Falk, S.J., Guo, L.Y., Sekulic, N., Smoak, E.M., Mani, T., Logsdon, G.A., Gupta, K., Jansen, L.E., Van Duyne, G.D., Vinogradov, S.A., et al. (2015). Chromosomes. CENP-C reshapes and stabilizes CENP-A nucleosomes at the centromere. Science *348*, 699–703. https://doi.org/10.1126/science.1259308.

49. Trazzi, S., Perini, G., Bernardoni, R., Zoli, M., Reese, J.C., Musacchio, A., and Della Valle, G. (2009). The C-terminal domain of CENP-C displays multiple and critical functions for mammalian centromere formation. PLoS One *4,* e5832. https://doi.org/10.1371/journal.pone.0005832.

50. Joseph, P.R., Poluri, K.M., Gangavarapu, P., Rajagopalan, L., Raghuwanshi, S., Richardson, R.M., Garofalo, R.P., and Rajarathnam, K. (2013). Proline substitution of dimer interface beta-strand residues as a strategy for the design of functional monomeric proteins. Biophys. J. *105*, 1491–1501. https://doi.org/10.1016/j.bpj.2013.08.008.

51. Clackson, T., Yang, W., Rozamus, L.W., Hatada, M., Amara, J.F., Rollins, C.T., Stevenson, L.F., Magari, S.R., Wood, S.A., Courage, N.L., et al. (1998). Redesigning an FKBP-ligand interface to generate chemical dimerizers with novel specificity. Proc. Natl. Acad. Sci. USA *95*, 10437–10442. https://doi.org/10.1073/pnas.95.18.10437.

52. Takamatsu, S., Onoguchi, K., Onomoto, K., Narita, R., Takahasi, K., Ishidate, F., Fujiwara, T.K., Yoneyama, M., Kato, H., and Fujita, T. (2013). Functional characterization of domains of IPS-1 using an inducible oligomerization system. PLoS One *8,* e53578. https://doi.org/10.1371/journal.pone.0053578.

53. Blower, M.D., Sullivan, B.A., and Karpen, G.H. (2002). Conserved organization of centromeric chromatin in flies and humans. Dev. Cell *2*, 319–330.

54. Sullivan, B.A., Blower, M.D., and Karpen, G.H. (2001). Determining centromere identity: cyclical stories and forking paths. Nat. Rev. Genet. *2*, 584–596. https://doi.org/10.1038/35084512.

55. Sullivan, B.A., and Karpen, G.H. (2004). Centromeric chromatin exhibits a histone modification pattern that is distinct from both euchromatin and heterochromatin. Nat. Struct. Mol. Biol. *11*, 1076–1083. https://doi.org/10.1038/nsmb845.

56. Ribeiro, S.A., Vagnarelli, P., Dong, Y., Hori, T., McEwen, B.F., Fukagawa, T., Flors, C., and Earnshaw, W.C. (2010). A super-resolution map of the vertebrate kinetochore. Proc. Natl. Acad. Sci. USA *107*, 10484–10489. https://doi.org/10.1073/pnas.1002325107.

57. Nishimura, K., Komiya, M., Hori, T., Itoh, T., and Fukagawa, T. (2019). 3D genomic architecture reveals that neocentromeres associate with heterochromatin regions. J. Cell Biol. *218*, 134–149. https://doi.org/10.1083/jcb.201805003.

58. Hagège, H., Klous, P., Braem, C., Splinter, E., Dekker, J., Cathala, G., de Laat, W., and Forné, T. (2007). Quantitative analysis of chromosome conformation capture assays (3C-qPCR). Nat. Protoc. *2*, 1722–1733. https://doi.org/10.1038/nprot.2007.243.

59. Shang, W.H., Hori, T., Martins, N.M., Toyoda, A., Misu, S., Monma, N., Hiratani, I., Maeshima, K., Ikeo, K., Fujiyama, A., et al. (2013). Chromosome engineering allows the efficient isolation of vertebrate neocentromeres. Dev. Cell *24*, 635–648. https://doi.org/10.1016/j.devcel.2013.02.009.

60. Shang, W.H., Hori, T., Toyoda, A., Kato, J., Popendorf, K., Sakakibara, Y., Fujiyama, A., and Fukagawa, T. (2010). Chickens possess centromeres with both extended tandem repeats and short non-tandem-repetitive sequences. Genome Res. *20*, 1219–1228. https://doi.org/10.1101/gr.106245.110.

61. Hori, T., Kagawa, N., Toyoda, A., Fujiyama, A., Misu, S., Monma, N., Makino, F., Ikeo, K., and Fukagawa, T. (2017). Constitutive centromere-associated network controls centromere drift in vertebrate cells. J. Cell Biol. *216*, 101–113. https://doi.org/10.1083/jcb.201605001.

62. Kato, H., Jiang, J., Zhou, B.R., Rozendaal, M., Feng, H., Ghirlando, R., Xiao, T.S., Straight, A.F., and Bai, Y. (2013). A conserved mechanism for centromeric nucleosome recognition by centromere protein CENP-C. Science *340*, 1110–1113. https://doi.org/10.1126/science.1235532.

63. Carroll, C.W., Silva, M.C., Godek, K.M., Jansen, L.E., and Straight, A.F. (2009). Centromere assembly requires the direct recognition of CENP-A nucleosomes by CENP-N. Nat. Cell Biol. *11*, 896–902. https://doi.org/10.1038/ncb1899.

64. Tian, T., Li, X., Liu, Y., Wang, C., Liu, X., Bi, G., Zhang, X., Yao, X., Zhou, Z.H., and Zang, J. (2018). Molecular basis for CENP-N recognition of CENP-A nucleosome on the human kinetochore. Cell Res. *28*, 374–378. https://doi.org/10.1038/cr.2018.13.

65. Chittori, S., Hong, J., Saunders, H., Feng, H., Ghirlando, R., Kelly, A.E., Bai, Y., and Subramaniam, S. (2018). Structural mechanisms of centromeric nucleosome recognition by the kinetochore protein CENP-N. Science *359*, 339–343. https://doi.org/10.1126/science.aar2781.

66. Maddox, P.S., Hyndman, F., Monen, J., Oegema, K., and Desai, A. (2007). Functional genomics identifies a Myb domain-containing protein family required for assembly of CENP-A chromatin. J. Cell Biol. *176*, 757–763. https://doi.org/10.1083/jcb.200701065.

67. Fujita, Y., Hayashi, T., Kiyomitsu, T., Toyoda, Y., Kokubu, A., Obuse, C., and Yanagida, M. (2007). Priming of centromere for CENP-A recruitment by human hMis18alpha, hMis18beta, and M18BP1. Dev. Cell *12*, 17–30. https://doi.org/10.1016/j.devcel.2006.11.002.

68. Moree, B., Meyer, C.B., Fuller, C.J., and Straight, A.F. (2011). CENP-C recruits M18BP1 to centromeres to promote CENP-A chromatin assembly. J. Cell Biol. *194*, 855–871. https://doi.org/10.1083/jcb.201106079.

69. Hori, T., Shang, W.H., Hara, M., Ariyoshi, M., Arimura, Y., Fujita, R., Kurumizaka, H., and Fukagawa, T. (2017). Association of M18BP1/KNL2 with CENP-A nucleosome is essential for centromere formation in non-mammalian vertebrates. Dev. Cell *42*, 181–189.e3. https://doi.org/10.1016/j.devcel.2017.06.019.

70. French, B.T., Westhorpe, F.G., Limouse, C., and Straight, A.F. (2017). Xenopus laevis M18BP1 directly binds existing CENP-A nucleosomes to promote centromeric chromatin assembly. Dev. Cell *42*, 190–199.e10. https://doi.org/10.1016/j.devcel.2017.06.021.

71. Kral, L. (2015). Possible identification of CENP-C in fish and the presence of the CENP-C motif in M18BP1 of vertebrates. F1000Res *4*, 474. https://doi.org/10.12688/f1000research.6823.2.

72. Sandmann, M., Talbert, P., Demidov, D., Kuhlmann, M., Rutten, T., Conrad, U., and Lermontova, I. (2017). Targeting of Arabidopsis KNL2 to centromeres depends on the conserved CENPC-k motif in its C terminus. Plant Cell *29*, 144–155. https://doi.org/10.1105/tpc.16.00720.

73. Jiang, H., Ariyoshi, M., Hori, T., Watanabe, R., Makino, F., Namba, K., and Fukagawa, T. (2023). The cryo-EM structure of the CENP-A nucleosome in complex with ggKNL2. EMBO J. *42,* e111965. https://doi.org/10.15252/embj.2022111965.

74. Dambacher, S., Deng, W., Hahn, M., Sadic, D., Fröhlich, J., Nuber, A., Hoischen, C., Diekmann, S., Leonhardt, H., and Schotta, G. (2012).

CENP-C facilitates the recruitment of M18BP1 to centromeric chromatin. Nucleus *3*, 101–110. https://doi.org/10.4161/nucl.18955.

75. McKinley, K.L., and Cheeseman, I.M. (2014). Polo-like kinase 1 licenses CENP-A deposition at centromeres. Cell *158*, 397–411. https://doi.org/10.1016/j.cell.2014.06.016.
76. French, B.T., and Straight, A.F. (2019). CDK phosphorylation of Xenopus laevis M18BP1 promotes its metaphase centromere localization. EMBO J. *38,* e100093. https://doi.org/10.15252/embj.2018100093.
77. Kim, J., Ishiguro, K., Nambu, A., Akiyoshi, B., Yokobayashi, S., Kagami, A., Ishiguro, T., Pendas, A.M., Takeda, N., Sakakibara, Y., et al. (2015). Meikin is a conserved regulator of meiosis-I-specific kinetochore function. Nature *517*, 466–471. https://doi.org/10.1038/nature14097.
78. Maier, N.K., Ma, J., Lampson, M.A., and Cheeseman, I.M. (2021). Separase cleaves the kinetochore protein Meikin at the meiosis I/II transition. Dev. Cell *56*, 2192–2206.e8. https://doi.org/10.1016/j.devcel.2021.06.019.
79. Ando, S., Yang, H., Nozaki, N., Okazaki, T., and Yoda, K. (2002). CENP-A, -B, and -C chromatin complex that contains the I-type alpha-satellite array constitutes the prekinetochore in HeLa cells. Mol. Cell. Biol. *22*, 2229–2241.
80. Mátés, L., Chuah, M.K., Belay, E., Jerchow, B., Manoj, N., Acosta-Sanchez, A., Grzela, D.P., Schmitt, A., Becker, K., Matrai, J., et al. (2009). Molecular evolution of a novel hyperactive Sleeping Beauty transposase enables robust stable gene transfer in vertebrates. Nat. Genet. *41*, 753–761. https://doi.org/10.1038/ng.343.
81. Cong, L., Ran, F.A., Cox, D., Lin, S., Barretto, R., Habib, N., Hsu, P.D., Wu, X., Jiang, W., Marraffini, L.A., and Zhang, F. (2013). Multiplex genome engineering using CRISPR/Cas systems. Science *339*, 819–823. https://doi.org/10.1126/science.1231143.
82. Schindelin, J., Arganda-Carreras, I., Frise, E., Kaynig, V., Longair, M., Pietzsch, T., Preibisch, S., Rueden, C., Saalfeld, S., Schmid, B., et al. (2012). Fiji: an open-source platform for biological-image analysis. Nat. Methods *9*, 676–682. https://doi.org/10.1038/nmeth.2019.
83. Pei, J., Tang, M., and Grishin, N.V. (2008). PROMALS3D web server for accurate multiple protein sequence and structure alignments. Nucleic Acids Res. *36*. W30–W34. https://doi.org/10.1093/nar/gkn322.
84. Kabsch, W. (2010). Xds. Acta Crystallogr. D Biol. Crystallogr. *66*, 125–132. https://doi.org/10.1107/S0907444909047337.
85. Vagin, A., and Teplyakov, A. (2010). Molecular replacement with MOLREP. Acta Crystallogr. D Biol. Crystallogr. *66*, 22–25. https://doi.org/10.1107/S0907444909042589.
86. Winn, M.D., Ballard, C.C., Cowtan, K.D., Dodson, E.J., Emsley, P., Evans, P.R., Keegan, R.M., Krissinel, E.B., Leslie, A.G., McCoy, A., et al. (2011). Overview of the CCP4 suite and current developments. Acta Crystallogr. D Biol. Crystallogr. *67*, 235–242. https://doi.org/10.1107/S0907444910045749.
87. Emsley, P., Lohkamp, B., Scott, W.G., and Cowtan, K. (2010). Features and development of coot. Acta Crystallogr. D Biol. Crystallogr. *66*, 486–501. https://doi.org/10.1107/S0907444910007493.
88. Murshudov, G.N., Vagin, A.A., Lebedev, A., Wilson, K.S., and Dodson, E.J. (1999). Efficient anisotropic refinement of macromolecular structures using FFT. Acta Crystallogr. D Biol. Crystallogr. *55*, 247–255. https://doi.org/10.1107/S090744499801405X.
89. Touw, W.G., Baakman, C., Black, J., te Beek, T.A., Krieger, E., Joosten, R.P., and Vriend, G. (2015). A series of PDB-related databanks for everyday needs. Nucleic Acids Res. *43*. D364–D368. https://doi.org/10.1093/nar/gku1028.
90. Harris, C.R., Millman, K.J., van der Walt, S.J., Gommers, R., Virtanen, P., Cournapeau, D., Wieser, E., Taylor, J., Berg, S., Smith, N.J., et al. (2020). Array programming with NumPy. Nature *585*, 357–362. https://doi.org/10.1038/s41586-020-2649-2.
91. Virtanen, P., Gommers, R., Oliphant, T.E., Haberland, M., Reddy, T., Cournapeau, D., Burovski, E., Peterson, P., Weckesser, W., Bright, J., et al. (2020). SciPy 1.0: fundamental algorithms for scientific computing in Python. Nat. Methods *17*, 261–272. https://doi.org/10.1038/s41592-019-0686-2.
92. Hunter, J.D. (2007). Matplotlib: A 2D graphics environment. Comput. Sci. Eng. *9*, 90–95. https://doi.org/10.1109/MCSE.2007.55.
93. Pedregosa, F., Varoquaux, G., Gramfort, A., Michel, V., Thirion, B., Grisel, O., Blondel, M., Prettenhofer, P., Weiss, R., Dubourg, V., et al. (2011). Scikit-learn: machine learning in Python. J. Mach. Learn. Res. *12*, 2825–2830.
94. Buerstedde, J.M., Reynaud, C.A., Humphries, E.H., Olson, W., Ewert, D.L., and Weill, J.C. (1990). Light chain gene conversion continues at high rate in an ALV-induced cell line. EMBO J. *9*, 921–927.
95. Pettersen, E.F., Goddard, T.D., Huang, C.C., Meng, E.C., Couch, G.S., Croll, T.I., Morris, J.H., and Ferrin, T.E. (2021). UCSF ChimeraX: structure visualization for researchers, educators, and developers. Protein Sci. *30*, 70–82. https://doi.org/10.1002/pro.3943.
96. Balzarotti, F., Eilers, Y., Gwosch, K.C., Gynnå, A.H., Westphal, V., Stefani, F.D., Elf, J., and Hell, S.W. (2017). Nanometer resolution imaging and tracking of fluorescent molecules with minimal photon fluxes. Science *355*, 606–612. https://doi.org/10.1126/science.aak9913.
97. Schmidt, R., Weihs, T., Wurm, C.A., Jansen, I., Rehman, J., Sahl, S.J., and Hell, S.W. (2021). MINFLUX nanometer-scale 3D imaging and microsecond-range tracking on a common fluorescence microscope. Nat. Commun. *12*, 1478. https://doi.org/10.1038/s41467-021-21652-z.

STAR★METHODS

KEY RESOURCES TABLE

REAGENT or RESOURCE	SOURCE	IDENTIFIER
Antibodies		
Rabbit polyclonal anti-chicken CENP-C	Fukagawa et al.[33]	RRID: AB_2665548
Rabbit polyclonal anti-GFP	MBL	Cat#598; RRID: AB_591819
Mouse monoclonal Anti-α-Tubulin antibody	Sigma	Cat#T9026; RRID: AB_477593
Guinea pig polyclonal anti-human CENP-C (hCENP-C)	Ando et al.[79]	N/A
Rat monoclonal anti-RFP [5F8]	ChromoTek	Cat#5f8-100; RRID:AB_2336064
Rabbit polyclonal anti-chicken CENP-T	Hori et al.[10]	RRID: AB_2665551
Rabbit polyclonal anti-chicken CENP-H	Fukagawa et al.[42]	RRID: AB_2665549
Mouse monoclonal Anti-human CENP-A antibody	Ando et al.[79]	N/A
Rabbit monoclonal Anti-human Cyclin B1 antibody	Cell Signaling Technology	Cat#12231; RRID: AB_2783553
HRP-conjugated anti-Rabbit IgG	Jackson ImmunoResearch Labs	Cat# 111-035-144; RRID: AB_2307391
HRP-conjugated anti-mouse IgG	Jackson ImmunoResearch Labs	Cat# 115-035-003; RRID: AB_10015289
HRP-conjugated anti-Guinea pig IgG	Jackson ImmunoResearch Labs	Cat#106-035-003; RRID: AB_2337402
HRP-conjugated anti-Rat IgG	Jackson ImmunoResearch Labs	Cat#112-035-003; RRID: AB_2338128
Alexa Fluor 647-conjugated anti Rabbit IgG	Jackson ImmunoResearch Labs	Cat#111-607-008; RRID: AB_2632470
Alexa Fluor 647-conjugated anti Mouse IgG	Jackson ImmunoResearch Labs	Cat#115-607-003; RRID: AB_2338931
Cy3-conjugated anti-rabbit IgG	Jackson ImmunoResearch Labs	Cat#211-165-109; RRID: AB_2339158
Purified Mouse Anti-BrdU	BD Biosciences	Cat#347580; RRID: AB_10015219
FITC-conjugated anti-mouse IgG	Jackson ImmunoResearch Labs	Cat#315-095-003; RRID: AB_2340106
Bacterial and virus strains		
Escherichia coli: Rosetta2 (DE3)	Merck	Cat# 71400
Chemicals, peptides, and recombinant proteins		
Signal Enhancer HIKARI for Western Blotting and ELISA	Nacalai Tesque	Cat# 02270-81
ECL Prime	Cytiva	Cat# RPN2232
VECTASHIELD	Vector Laboratories	Cat# H-1000-10
16% PFA	Electron Microscopy Sciences	Cat# 15710
cOmplete, EDTA-free Protease Inhibitor Cocktail	Roche	Cat# 11873580001
HindIII (high conc.)	NIPPON GENE	Cat# 311-01761
T4 DNA Ligase	Promega	Cat# M1794
EcoRI (high conc.)	NIPPON GENE	Cat# 314-01751
CENP-C^{CBD} (166-324)	This paper	N/A
CENP-C$^{C\text{-}term}$ (677-864)	This paper	N/A
Mini-CENP-C ([166-324]-[677-864])	This paper	N/A
MBP-CENP-L (aa 13-344)/ MBP-CENP-N$^{C\text{-}term}$ (aa 252-354) complex	Nagpal et al.[37]	N/A
MBP-AviTag-His6	Tonia Rex lab	N/A
Mif2p$^{C\text{-}term}$ (307-549)	This paper	NA
CENP-C$^{C\text{-}term\ PP}$ (677-864 F756P/F757P)	This paper	NA
hCENP-C$^{C\text{-}term}$ WT (760-943)	This paper	N/A
hCENP-C$^{C\text{-}term}$ ΔOI (760-943 Δ846-851)	This paper	N/A
human rhinovirus 3C (HRV3C) protease	Ariyoshi et al.[43]	N/A
Glucose Oxidase	Sigma	Cat# G2133-250KU

(*Continued on next page*)

Continued

REAGENT or RESOURCE	SOURCE	IDENTIFIER
Catalase	FUJIFILM	Cat# 035-12903
150 nm gold beads	BBI Solutions	Cat# EM.GC150/4
Critical commercial assays		
Qubit dsDNA HS Assay Kit	Thermo Fisher Scientific	Cat# Q32851
TaqMan Fast Advanced Master Mix	Thermo Fisher Scientific	Cat# 4444557
iDimerize Inducible Homodimer System	Takara	Cat# 635068
Deposited data		
Chicken CENP-C Cupin domain	This paper	PDB: 7X85
Schizosaccharomyces pombe Cnp3 Cupin domain	Chik et al.[39]	PDB: 6O2D
Drosophila melanogaster CENP-C Cupin domain	Chik et al.[39]	PDB: 6O2K
Saccharomyces cerevisiae Mif2p Cupin domain	Cohen et al.[38]	PDB: 2VPV
Chicken CENP-C	NCBI	NCBI Reference Sequence: NP_001376225.2
Human CENP-C	NCBI	NCBI Reference Sequence: NP_001803
Mouse CENP-C	NCBI	NCBI Reference Sequence: NP_031709
Xenopus laevis CENP-C	NCBI	NCBI Reference Sequence: NP_001159485
Drosophila melanogaster CENP-C	NCBI	NCBI Reference Sequence: NP_731254
Schizosaccharomyces pombe Cnp3	NCBI	NCBI Reference Sequence: NP_001342907
Saccharomyces cerevisiae Mif2p	Uniport	UniProtKB: P35201
Chicken genome sequence galGal4	USCS Genome Browser	genome-asia.ucsc.edu/cgi-bin/hgGateway?org=Chicken&redirect=manual&source=www.genome.ucsc.edu
Chicken genome sequence galGal4	USCS Genome Browser	genome-asia.ucsc.edu/cgi-bin/hgGateway?org=Chicken&redirect=manual&source=www.genome.ucsc.edu
Original data	This paper	Mendeley Data: https://doi.org/10.17632/k6jnkjbd8k.1
Experimental models: Cell lines		
Chicken: DT40 cKO-CENP-C cells	Kwon et al.[41]	N/A
Chicken: DT40 cKO-CENP-C/GFP-CENP-C^{FL} cells	Hara et al.[35]	N/A
Chicken: DT40 cKO-CENP-C/GFP-CENP-$C^{\Delta CBD}$ (Δ166-324) cells	This paper	N/A
Chicken: DT40 cKO-CENP-C/GFP-CENP-$C^{\Delta C\text{-}term}$ (Δ677-864) cells	This paper	N/A
Chicken: DT40 cKO-CENP-C/GFP-CENP-$C^{\Delta Mid\text{-}DR}$ (Δ325-676) cells	This paper	N/A
Chicken: DT40 cKO-CENP-C/GFP-Mini-CENP-C ([166-324]-[677-864]) cells	This paper	N/A
Chicken: DT40 cKO-CENP-C/GFP-CENP-$C^{[166\text{-}324]\text{-}[722\text{-}864]}$ cells	This paper	N/A
Chicken: DT40 cKO-CENP-C/GFP-CENP-$C^{\Delta OI}$ (Δ754-760) cells	This paper	N/A
Chicken: DT40 cKO-CENP-C/GFP-CENP-C^{PP} (F756P/F757P) cells	This paper	N/A
Chicken: DT40 cKO-CENP-C/GFP-CENP-C^{CBD} (166-324) cells	This paper	N/A
Chicken: DT40 cKO-CENP-C/GFP-CENP-$C^{CBD\text{-}1xDmrB}$ ([166-324]-[677-724]-1xDmrB) cells	This paper	N/A
Chicken: DT40 cKO-CENP-C/GFP-CENP-$C^{CBD\text{-}3xDmrB}$ ([166-324]-[677-724]-3xDmrB) cells	This paper	N/A

(*Continued on next page*)

Continued

REAGENT or RESOURCE	SOURCE	IDENTIFIER
Chicken: DT40 cKO-CENP-C/GFP-CENP-C^{CBD} (166-324)/mRFP-CENP-$C^{C\text{-}term}$ (677-864) cells	This paper	N/A
Chicken: DT40 cKO-CENP-C/GFP-CENP-C^{Cupin_Mut} (Y799A/H843A) cells	This paper	N/A
Chicken: DT40 cKO-CENP-C/GFP-CENP-$C^{\Delta DH}$ (Δ725-753) cells	This paper	N/A
Chicken: DT40 cKO-CENP-C/GFP-CENP-$C^{\Delta DH/Cupin\_Mut}$ (Δ725-753Y799A/H843A) cells	This paper	N/A
Chicken: DT40 cKO-CENP-C/mScarlet-CENP-N cells	This paper	N/A
Chicken: DT40 cKO-CENP-C/mScarlet-CENP N/GFP-CENP-C^{FL} cells	This paper	N/A
Chicken: DT40 cKO-CENP-C/mScarlet-CENP-N/GFP-CENP-$C^{\Delta CBD}$ (Δ166-324) cells	This paper	N/A
Chicken: DT40 cKO-CENP-C/mScarlet-CENP-N/GFP-CENP-$C^{\Delta C\text{-}term}$ (Δ677-864) cells	This paper	N/A
Chicken: DT40 cKO-CENP-C/mScarlet-CENP-N/GFP-Mini-CENP-C ([166-324]-[677-864]) cells	This paper	N/A
Chicken: DT40 cKO-CENP-C/mScarlet-CENP-N/GFP-CENP-$C^{\Delta OI}$ (Δ754-760) cells	This paper	N/A
Chicken: DT40 cKO-CENP-C/mScarlet-CENP-N/GFP-CENP-$C^{CBD\text{-}1xDmrB}$ ([166-324]-[677-724]-1xDmrB) cells	This paper	N/A
Chicken: DT40 cKO-CENP-C/mScarlet-CENP-N/GFP-CENP-$C^{CBD\text{-}3xDmrB}$ ([166-324]-[677-724]-3xDmrB) cells	This paper	N/A
Chicken: DT40 cKO-CENP-C/mScarlet-CENP-A cells	This paper	N/A
Chicken: DT40 cKO-CENP-C/mScarlet-CENP-A/GFP-CENP-C^{FL} cells	This paper	N/A
Chicken: DT40 cKO-CENP-C/mScarlet-CENP-A/GFP-Mini-CENP-C ([166-324]-[677-864]) cells	This paper	N/A
Chicken: DT40 CL18/GFP-CENP-C^{FL} cells	This paper	N/A
Chicken: DT40 CL18/GFP-Mini-CENP-C ([166-324]-[677-864]) cells	This paper	N/A
Chicken: DT40 CENP-C KO/GFP-CENP-C^{FL} cells #1	This paper	N/A
Chicken: DT40 CENP-C KO/GFP-CENP-C^{FL} cells #2	This paper	N/A
Chicken: DT40 CENP-C KO/GFP-Mini-CENP-C ([166-324]-[677-864]) cells #1	This paper	N/A
Chicken: DT40 CENP-C KO/GFP-Mini-CENP-C ([166-324]-[677-864]) cells #2	This paper	N/A
Chicken: DT40 cKO-CENP-C/GFP-1xDmrB cells	This paper	N/A
Chicken: DT40 cKO-CENP-C/GFP-3xDmrB cells	This paper	N/A
Chicken: DT40 Z#3 cells (WT control cells for 3C-qPCR)	Shang et al.[59]	N/A
Chicken: DT40 #1320 cells (neocentromere cells)	Shang et al.[59]	N/A
Chicken: DT40 #1320/CENP-C-AID cells	Nishimura et al.[57]	N/A
Chicken: DT40 #1320/CENP-H-AID cells	Nishimura et al.[57]	N/A
Human: hTERT-RPE1 hCENP-C-AID-mCherry cells	Watanabe et al.[36]	N/A

(*Continued on next page*)

Continued

REAGENT or RESOURCE	SOURCE	IDENTIFIER
Human: hTERT-RPE1 hCENP-C-AID-mCherry/ GFP-hCENP-C FL cells	Watanabe et al.[36]	N/A
Human: hTERT-RPE1 hCENP-C-AID-mCherry/ GFP-hCENP-C$^{\Delta OI}$ (Δ846-851) cells #1	This paper	N/A
Human: hTERT-RPE1 hCENP-C-AID-mCherry/ GFP-hCENP-C$^{\Delta OI}$ (Δ846-851) cells #2	This paper	N/A
Oligonucleotides		
See Table S2 for 3C-qPCR primers	This paper	N/A
TaqMan MGB (5'-FAM) probe #1320 (neocentromere): TGTTTTGATTACACTTGCTGCT	This paper	N/A
TaqMan MGB (5'-FAM) probe ChrZ centromere region 1: AACCTTTGATCAGTCTTC	This paper	N/A
TaqMan MGB (5'-FAM) probe ChrZ centromere region 2: ACAGCCTGTTCTTTCAG	This paper	N/A
TaqMan MGB (5'-FAM) probe FAM ChrZ lading control (SMC5 locus): CGTGCTGCGAATAC	This paper	N/A
CENP-C KO primer F1: GCAGGGAGACTGCTCTCTAAGTG	This paper	N/A
CENP-C KO primer F2: GTTTGTCCAAACTCATCAATGTATC	This paper	N/A
CENP-C KO primer F3: AGACAGAATAAAACGCACGGTG	This paper	N/A
CENP-C KO primer R1: CTGACTGACAAGATGCTGTC	This paper	N/A
CENP-C KO primer R2: AGAACGTGGGGCTCACCTCGAC	This paper	N/A
CENP-C KO primer R3: TTGCCTGCCTATCTCGTCTGA	This paper	N/A
Recombinant DNA		
pEGFP-C3	Clontech	Cat# 6082-1
pEGFP-C3-CENP-C^{FL}	Hara et al.[35]	N/A
pEGFP-C3-CENP-C$^{\Delta CBD}$ (Δ166-324)	This paper	N/A
pEGFP-C3-CENP-C$^{\Delta C\text{-}term}$ (Δ677-864)	This paper	N/A
pEGFP-C3-CENP-C$^{\Delta Mid\text{-}DR}$ (Δ325-676)	This paper	N/A
pEGFP-C3-Mini-CENP-C ([166-324]-[677-864])	This paper	N/A
pEGFP-C3-CENP-C$^{[166\text{-}324]\text{-}[722\text{-}864]}$	This paper	N/A
pEGFP-C3-CENP-C$^{\Delta OI}$ (Δ754-760)	This paper	N/A
pEGFP-C3-CENP-C^{PP} (F756P/F757P)	This paper	N/A
pEGFP-C3-CENP-C^{Cupin_Mut} (Y799A/H843)	This paper	N/A
pEGFP-C3-CENP-C$^{\Delta DH}$ (Δ725-753)	This paper	N/A
pEGFP-C3-CENP-C$^{\Delta DH/Cupin_Mut}$ (Δ725-753/Y799A/H843)	This paper	N/A
pEGFP-C3-CENP-C^{CBD} (166-324)	This paper	N/A
pmRFP-C3-CENP-C$^{C\text{-}term}$ (677-864)	This paper	N/A
pEGFP-C3-1xDmrB	This paper	N/A
pEGFP-C3-3xDmrB	This paper	N/A
pEGFP-C3- CENP-C$^{CBD\text{-}1xDmrB}$ ([166-324]-[677-724]-1xDmrB)	This paper	N/A

(*Continued on next page*)

Continued

REAGENT or RESOURCE	SOURCE	IDENTIFIER
pEGFP-C3- CENP-C$^{CBD\text{-}3xDmrB}$ ([166-324]-[677-724]-3xDmrB)	This paper	N/A
pT2/HB	Perry Hackett lab	Addgene plasmid # 26557
pT2/HB-hCENP-C$^{\Delta OI}$ (Δ848-854)	This paper	N/A
pCMV (CAT) T7-SB100	Mates et al.[80]	Addgene plasmid # 34879
pBS-CENP-N(Knock in homology arm)-mScarlet-CENP-N-BsR	This paper	N/A
pBS-CENP-N(Knock in homology arms)-mScarlet-CENP-N-Ecogpt	This paper	N/A
pX335-U6-Chimeric_BB-CBh-hSpCas9n(D10A)	Cong et al.[81]	Addgene Plasmid #42335
pX335-CENP-N	This paper	N/A
pBS-ACTB(Knock in homology arms)-mScarlet-CENP-A-IRES-Ecogpt	This paper	N/A
pX335-ACTB	Hara et al.[35]	N/A
pBS-CENP-C KO-PuroR	This paper	N/A
pBS-CENP-C KO-BsR	This paper	N/A
pX330-U6-Chimeric_BB-CBh-hSpCas9	Cong et al.[81]	Addgene Plasmid #42230
pX330-CENP-C KO #1	This paper	N/A
pX330-CENP-C KO #2	This paper	N/A
pGEX-6P-1	Cytiva	Cat# 27-4597-01
pGEX-6P-1-CENP-C$^{C\text{-}term}$ (677-864)	This paper	N/A
pGEX-6P-1-Mif2p$^{C\text{-}term}$ (307-549)	This paper	N/A
pGEX-6P-1-CENP-C$^{C\text{-}term\ PP}$ (677-864 F756P/F757P)	This paper	N/A
pGEX-6P-1-hCENP-C$^{C\text{-}term}$ (760-943)	This paper	N/A
pGEX-6P-1-hCENP-C$^{C\text{-}term\Delta OI}$ (760-943 Δ846-851)	This paper	N/A
pGEX-6P-1-CENP-C^{CBD} (166-324)	This paper	N/A
pGEX-6P-1-Mini-CENP-C ([166-324]-[677-864])	This paper	N/A
pRSFDuet-MBP-CENP-N$^{C\text{-}term}$-MBP-CENP-L (CENP-N aa 252-344, CENP-L aa 13-344)	Nagpal et al.[37]	N/A
pMal-T-Avi-His/BirA	Tonia Rex lab	Addgene plasmid # 102962
pGEM-T Easy	Promega	Cat# A1360
pGEM-T Easy NeoCen#1320 A	This paper	N/A
pGEM-T Easy NeoCen#1320 B	This paper	N/A
pGEM-T Easy NeoCen#1320 C	This paper	N/A
pGEM-T Easy NeoCen#1320 D	This paper	N/A
pGEM-T Easy ChrZ centromere A	This paper	N/A
pGEM-T Easy ChrZ centromere B	This paper	N/A
pGEM-T Easy ChrZ centromere C	This paper	N/A
pGEM-T Easy ChrZ centromere D	This paper	N/A
pGEM-T Easy ChrZ centromere E	This paper	N/A
pGEM-T Easy ChrZ centromere F	This paper	N/A
pGEM-T Easy ChrZ centromere G	This paper	N/A
pGEM-T Easy ChrZ centromere H	This paper	N/A
pGEM-T Easy ChrZ centromere I	This paper	N/A

(*Continued on next page*)

Continued

REAGENT or RESOURCE	SOURCE	IDENTIFIER
Software and algorithms		
Image Lab 6.1.0	BioRad	RRID:SCR_014210
Photoshop 2023	Adobe	RRID:SCR_014199
Illustrator 2023	Adobe	RRID:SCR_010279
NIS-elements AR 4.8	Nikon	RRID:SCR_014329
Fiji	[82]	RRID:SCR_002285
Imaris 9.2.1	Bitplane	RRID:SCR_007370
Prism7	GraphPad	RRID:SCR_002798
Microsoft Excel for Mac	Microsoft	RRID:SCR_016137
guavaSoft 2.7	Merck	https://www.emdmillipore.com/US/en/20130828_204624?bd=1
InCyte 3.1	Merck	https://www.emdmillipore.com/US/en/20130828_204624
PROMALS3	Schindelin et al.[83]	RRID:SCR_018161
XDS	Kabsch[84]	RRID:SCR_015652
Molrep (CCP4 suite)	Vagin and Teplyakov,[85] Winn et al.[86]	https://www.ccp4.ac.uk/html/molrep.html
Coot	Emsley et al.[87]	RRID:SCR_014222
REFMAC	Murshudov et al.[88]	RRID:SCR_014225
DSSP	Touw et al.[89]	https://swift.cmbi.umcn.nl/gv/dssp/
PyMOL	Schrödinger, LLC	RRID:SCR_000305
SoftWoRx software (v7.0.0)	Cytiva	RRID:SCR_019157
numpy 1.21.5	Harris et al.[90]	https://numpy.org/
scipy 1.7.3	Virtanen et al.[91]	https://www.scipy.org/
matplotlib 3.5.1	Hunter[92]	https://matplotlib.org/
scikit-learn 1.0.2	Pedregosa et al.[93]	https://scikit-learn.org/
QuantStudio Design and Analysis Software v1.5.1	Thermo Fisher Scientific	RRID:SCR_020238
IUPred3	Erdos et al.[46]	RRID:SCR_014632

RESOURCE AVAILABILITY

Lead contact

Further information and requests for resources and reagents should be directed to and will be fulfilled by the Lead Contact, Tatsuo Fukagawa (fukagawa.tatsuo.fbs@osaka-u.ac.jp).

Materials availability

All unique reagents generated in this study are available from the lead contact with a completed Materials Transfer Agreement.

Data and code availability

- The coordinates and structure factors have been deposited at PDB and are publicly available as of the date of publication. Accession numbers are listed in the key resources table. Original data have been deposited at Mendeley and are publicly available as of the date of publication. The DOI is listed in the key resources table.
- This paper does not report original code.
- Any additional information required to reanalyze the data reported in this paper is available from the lead contact upon request.

EXPERIMENTAL MODEL AND SUBJECT DETAILS

Chicken DT40 cells

A chicken DT40 cell line CL18 was used as the wild-type (WT) cell.[94] DT40 cells were cultured at 38.5°C in DMEM medium (Nacalai Tesque) supplemented with 10% fetal bovine serum (FBS; Sigma), 1% chicken serum (Thermo Fisher Scientific), and Penicillin-Streptomycin (Thermo Fisher Scientific) (DT40 culture medium).

The chicken CENP-C conditional knockout (cKO-CENP-C) DT40 cell line was described before.[41] The cKO-CENP-C cell line expressing GFP-CENP-C full-length (FL: cKO-CENP-C/GFP-CENP-C^{FL}) was described before.[35] To conditionally knockout CENP-C, the cells were cultured in DT40 culture medium containing 2 μg/ml tetracycline (Tet, Sigma).

The cKO-CENP-C cell lines expressing GFP-CENP-C ΔCBD (Δ166-324), ΔC-term (Δ677-864) or ΔMid-DR (Δ325-676) (cKO-CENP-C/GFP-CENP-C ΔCBD, ΔC-term, ΔMid-DR)[37] were re-established in this study by transfection of a plasmid encoding GFP-fused CENP-C ΔCBD, ΔC-term or ΔMid-DR and a neomycin resistance gene into cKO-CENP-C cells. Briefly, plasmid constructs were linearized by appropriate restriction enzymes and transfected into DT40 cells using Gene Pulser II electroporator (Bio-Rad). The transfected cells were selected in DT40 culture medium containing 2 mg/ml G418 (Santa Cruz Biotechnology).

The cKO-CENP-C cell lines expressing GFP-CENP-C Mini-CENP-C ([166-324]-[677-864]), [166-324]-[722-864], ΔOI (Δ754-760), PP (F756P/F757P), CBD (166-324), CBD-1xDmrB ([166-324]-[677-724]-1xDmrB), CBD-3xDmrB ([166-324]-[677-724]-3xDmrB), Cupin_Mut (Y799A/H843), ΔDH (Δ725-753), or ΔDH/Cupin_Mut (Δ725-753/Y799A/H843) were generated by transfection of a plasmid encoding GFP-fused CENP-C with indicated mutations as described above. (cKO-CENP-C/GFP-Mini-CENP-C, cKO-CENP-C/GFP-CENP-C ΔOI, PP, CBD, CBD-1xDmrB, CBD-3xDmrB, Cupin_Mut, ΔDH, ΔDH/Cupin_Mut).

To generate CENP-C knockout (CENP-C KO) cells expressing GFP-CENP-C^{FL} or GFP-Mini-CENP-C, first, a plasmid encoding GFP-CENP-C^{FL} or GFP-Mini-CENP-C and a neomycin resistance gene was transfected into CL18 (Wild-type) cells as described above. The transfected cells were selected in DT40 culture medium containing 2 mg/ml G418 (Santa Cruz Biotechnology). Then, endogenous CENP-C alleles in CL18/GFP-CENP-C^{FL} and CL18/GFP-Mini-CENP-C cells were knocked out by CRISPR-Cas9-mediated homology-directed repair (HDR). Briefly, the cells were transfected with plasmids, pX330 (pX330-U6-Chimeric_BB-CBh-hSpCas9, a gift from Feng Zhang, Addgene plasmid # 422350)[81]) with CENP-C KO gRNA #1, pX330 with CENP-C KO gRNA #2, and donor plasmids encoding a drug resistance gene expression cassette (PuroR or BsR) between 5' and 3' homology arms, using the Neon Transfection System (Thermo Fisher Scientific). The transfected cells were selected in DT40 culture medium containing 0.5 μg/ml Puromycin (Tokyo Chemical Industry) and 25 μg/ml Blasticidin S (FUJIFILUM). (CENP-C KO/GFP-CENP-C^{FL}, CENP-C KO/GFP-Mini-CENP-C).

To generate a cKO-CENP-C cell line expressing both GFP-CENP-C^{CBD} and mRFP-fused CENP-C$^{C\text{-}term}$, a plasmid encoding mRFP-fused CENP-C$^{C\text{-}term}$ was transfected with a plasmid encoding *Egogpt* gene into the cKO-CENP-C cell line expressing GFP-CENP-C^{CBD} using Gene Pulser II electroporator (Bio-Rad) as described above. The transfected cells were selected in DT40 culture medium containing 25 μg/ml Mycophenolic acid (Tokyo Chemical Industry) and 125 μg/ml Xanthine (Sigma). (cKO-CENP-C/GFP- CENP-C^{CBD}/mRFP-CENP-C$^{C\text{-}term}$).

To express mScarlet-fused chicken CENP-N under the control of endogenous CENP-N promoter, mScarlet-CENP-N cDNA was integrated into endogenous CENP-N locus using CRISPR/Cas9 -mediated HDR. cKO-CENP-C cell lines expressing indicated GFP-CENP-C protein were transfected with a plasmid encoding SpCas9 nickase (D10A) (pX335-U6-Chimeric_BB-CBh-hSpCas9n(D10A): a gift from Feng Zhang, Addgene plasmid # 42335)[81] and gRNA sequence for the CENP-N locus together with donor plasmids, which contained mScarlet-CENP-N cDNA and a drug resistance gene expression cassette (BsR or Ecogpt) between 5' and 3' homology arms (approximately 1 kb each) franking CENP-N start codon using Neon Transfection System (Thermo Fisher Scientific). The targeted cells were selected in DT40 culture medium containing 25 μg/ml Blasticidin S (FUJIFILUM), 25 μg/ml Mycophenolic acid and 125 μg/ml Xanthine. (cKO-CENP-C/mScarlet-CENP-N, cKO-CENP-C/mScarlet-CENP-N/GFP-CENP-C FL, ΔCBD, ΔC-term, Mini-CENP-C, ΔOI, CBD-1xDmrB, CBD-3xDmrB).

To express mScarlet-fused chicken CENP-A under the control of endogenous beta-actin (ACTB) promoter, mScarlet-CENP-A cDNA was integrated into the endogenous ACTB locus using CRISPR/Cas9-mdeiated HDR as previously described.[35] cKO-CENP-C cell lines expressing indicated GFP-CENP-C protein were transfected with the pX335 with gRNA sequence for ACTB[35] and a donor plasmid, which contained mScarlet-CENP-A cDNA and Ecogpt gene expression cassette between 5' and 3' homology arms (approximately 1 kb each) franking ACTB start codon using the Neon Transfection System (Thermo Fisher Scientific). The targeted cells were selected in DT40 culture medium containing 25μg/ml Mycophenolic acid and 125 μg/ml Xanthine. (cKO-CENP-C/mScarlet-CENP-A, cKO-CENP-C/mScarlet-CENP-A/GFP-CENP-C^{FL}, cKO-CENP-C/mScarlet-CENP-A/GFP-Mini-CENP-C).

cKO-CENP-C cells expressing GFP-1xDmrB or GFP-3xDmrB were generated by transfection of a plasmid encoding GFP-fused 1xDmrB or 3xDmrB as described above. (cKO-CENP-C/GFP-1xDmrB, cKO-CENP-C/GFP-3xDmrB).

To induce dimerization or oligomerization of 1xDmrB or 3xDmrB-fused proteins, respectively, cKO-CENP-C cells expressing these proteins were treated with 100 nM B/B Homodimerizer (Takara).

Human RPE-1 cells

RPE-1 cells were cultured at 37°C in DMEM medium (Nacalai Tesque) supplemented with 10% FBS (Sigma) and Penicillin-Streptomycin (Thermo Fisher Scientific) (RPE-1 culture medium).

The RPE-1 cell line in which Human CENP-C (hCENP-C) protein was conditionally depleted by the auxin-inducible degron system was previously described (RPE-1 hCENP-C-AID cell).[36] The hCENP-C-AID cell line expressing GFP-fused hCENP-C^{FL} was also described in Watanabe et al.[36] To deplete the AID-tagged hCENP-C (hCENP-C-AID-mCherry), the cells were cultured in RPE-1 culture medium containing 200 μM IAA (indole-3-acetic acid, Sigma).

To establish RPE-1 hCENP-C-AID cell line expressing GFP-fused hCENP-C$^{\Delta OI}$ (Δ846-851), the GFP-fused hCENP-C$^{\Delta OI}$ cDNA was integrated into the genome using Sleeping Beauty transposon system[80] (RPE-1 hCENP-C-AID /GFP-hCENP-C$^{\Delta OI}$). Plasmid

constructs were transfected into RPE-1 hCENP-C-AID cells with Neon Transfection System. Since the transgene cassette has a neomycin resistance gene, the cell lines were selected in RPE-1 culture medium containing 500 μg/ml G418.

METHOD DETAILS

Cell counting

To count DT40 cell numbers, the culture was mixed with the same volume of 0.4% (w/v) Trypan Blue Solution (FUJIFILM) and the cell numbers were counted by Countess II (Thermo Fisher Scientific).

To count RPE-1 cell numbers, the cells were trypsinized with 2.5 g/l-Trypsin-1 mmol/l EDTA solution (Nacalai tesque) and suspended into RPE-1 culture medium. The cell suspension was mixed with the same volume of 0.4% (w/v) Trypan Blue Solution (FUJIFILM) and the cell numbers were counted by Countess II (Thermo Fisher Scientific).

Plasmid constructions

Chicken CENP-C full-length (FL) cDNA sequence (NCBI Reference Sequence: NP_001376225.2)[31] was cloned into pEGFP-C3 (Clontech) (pEGFP-C3-CENP-C^{FL}).[35] Disordered regions were analyzed by IUPred3.[46] To prepare GFP-fused CENP-C mutants, deletion or mutation was introduced into pEGFP-C3-CENP-C^{FL} (pEGFP-C3-CENP-C ΔCBD (Δ166-324), ΔC-term (Δ677-864), ΔMid-DR (Δ325-676), Mini-CENP-C ([166-324]-[677-864]), [166-324]-[722-864], ΔOI (Δ754-760), CBD (166-324), Cupin_Mut (Y799A/H843A), ΔDH (Δ725-753), ΔDH/Cupin_Mut (Δ725-753/Y799A/H843A)). CENP-C^{CBD} was cloned into pEGFP-C3 (pEGFP-C3-CENP-C^{CBD}). CENP-$C^{C\text{-}term}$ was cloned into pEGFP-C3 whose EGFP was replaced with mRFP (pmRFP-C3-CENP-$C^{C\text{-}term}$). Single or three tandem-repeated DmrB, an inducible homodimerization domain (Takara), was amplified by PCR and cloned into pEGFP-C3 plasmid (Clontech) (pEGFP-C3-1xDmrB, pEGFP-C3-3xDmrB). CENP-$C^{[166\text{-}324]\text{-}[677\text{-}724]}$ was amplified by PCR and cloned into pEGFP-C3-1xDmrB and pEGFP-C3-3xDmrB (pEGFP-C3-CENP-$C^{CBD\text{-}1xDmrB}$, pEGFP-C3-CENP-$C^{CBD\text{-}3xDmrB}$).

Chicken CENP-N cDNA-fused with mScarlet and a drug resistance gene expression cassette (BsR or Ecogpt) were cloned in a plasmid, which contains CENP-N homology arms for knock-in (pBS-CENP-N(Knock in homology arm)-mScarlet-CENP-N-BsR or -Ecogpt).

Chicken CENP-A cDNA-fused with mScarlet and a drug resistance gene expression cassette (Ecogpt) was cloned in a plasmid which contains ACTB homology arms for knock-in (pBS-ACTB(Knock in homology arms)-mScarlet-CENP-A-IRES-Ecogpt).

hCENP-C FL cDNA sequence was cloned into pEGFP-C3 (pEGFP-C3-hCENP-C^{FL}).[36] aa 846-851 (Oligomer interface, OI) was deleted from pEGFP-C3-hCENP-C^{FL} by PCR (pEGFP-C3-hCENP-$C^{\Delta OI}$). The GFP-hCENP-C expression cassette together with neomycin resistance gene cassette in the pEGFP-C3 plasmid was amplified by PCR and cloned into pT2/HB (a gift from Perry Hackett, Addgene plasmid # 26557), a plasmid used for Sleeping Beauty transposon system,[80] using InFusion HD (Takara) (pT2/HB-hCENP-$C^{\Delta OI}$). The plasmid was used with pCMV (CAT) T7-SB100 (a gift from Zsuzsanna Izsvak, Addgene plasmid # 34879).[80]

Chicken CENP-$C^{C\text{-}term}$, Chicken CENP-C^{CBD}, Mini-CENP-C or $Mif2p^{C\text{-}term}$ cDNA sequence was cloned into inserted pGEX-6P-1 (Cytiva) for bacterial protein expression (pGEX-6P-1-CENP-$C^{C\text{-}term}$, pGEX-6P-1-CENP-C^{CBD}, pGEX-6P-1- CENP-$C^{Mini\text{-}CENP\text{-}C}$, pGEX-6P-1-$Mif2p^{C\text{-}term}$). Proline substitutions of F756 and F757 (F756P/F757P) were introduced into pGEX-6P-1-CENP-C^{Cterm} using PCR (pGEX-6P-1-CENP-$C^{Cterm\ PP}$).

cDNA fragments of maltose binding protein (MBP)-chicken CENP-N C-terminal domain (aa 252-344) and MBP-TEV protease cleavage site-chicken CENP-L (aa13-344) were cloned into multiple cloning sites, MCS1 and MCS2 in pRSFDuet vector (Novagen), respectively, for bacterial co-expression (pRSFDuet-MBP-CENP-L/N).[37]

pMal-T-Avi-His/BirA was a gift from Tonia Rex (Addgene plasmid # 102962; http://n2t.net/addgene:102962; RRID: Addgene_102962).

hCENP-$C^{760\text{-}943}$ (hCENP-$C^{C\text{-}term}$) cDNA sequence was cloned into pGEX-6P-1 (Cytiva) for bacterial protein expression (pGEX-6P-1-hCENP-$C^{C\text{-}term}$). Amino acid residues 846-851 were deleted from pGEX-hCENP-$C^{C\text{-}term}$ by PCR (pGEX-6P-1-hCENP-$C^{C\text{-}term\Delta OI}$).

For the 3C-qPCR standards, the ligated chimeric DNA fragments of target regions in the 3C library were amplified and cloned into pGEM-T Easy (Promega).

Immunoblotting

DT40 cells were harvested, washed with PBS, and suspended in 1xLSB (Laemmli sample buffer) (final $1x10^4$ cells/μl), followed by sonication and heating for 5 min at 96°C. In Figure S6C, insoluble fractions of DT40 cells were examined; DT40 cells were harvested, and washed with PBS twice, followed by another wash with TMS (10 mM Tris-HCl pH 7.5, 5 mM $MgCl_2$, 0.25 M sucrose). The cells were suspended in TMS supplemented with 0.5% Triton X-100 (TMS-Triton) and incubated for 5 min on ice. After centrifugation, the precipitates were denatured by adding 1xLSB, sonication, and heating for 5 min at 96°C. Proteins were separated on SuperSep Ace, 5-20% (FUJIFILM), and transferred to Immobilon-P (Merck) using HorizeBLOT (ATTO).

RPE-1 cells were trypsinized and harvested, washed with PBS, and suspended in 1xLSB (Laemmli sample buffer) (final $1x10^4$ cells/μl) followed by sonication and heating for 5 min at 96°C. Proteins were separated on SuperSep Ace, 5-20% (FUJIFILM), and transferred to Immobilon-P (Merck) using HorizeBLOT (ATTO).

Primary antibodies used in this study were rabbit anti-chicken CENP-C,[33] rabbit anti-GFP (MBL), mouse anti-alpha tubulin (Sigma), guinea pig anti-hCENP-C,[79] rat anti-RFP (Chromotek), rabbit anti-chicken CENP-H,[42] and rabbit anti-chicken CENP-T.[10] Secondary

antibodies were HRP-conjugated anti-Rabbit IgG (Jackson Immuno Research), HRP-conjugated anti-Mouse IgG (Jackson ImmunoResearch), HRP-conjugated anti-Rat IgG (Jackson ImmunoResearch), and HRP-conjugated anti-guinea pig (Sigma). To increase sensitivity and specificity, Signal Enhancer Hikari (Nacalai Tesque) was used to dilute all antibodies except for anti-alpha tubulin (5% skim milk in TBS 0.05% tween) and HRP-conjugated anti-mouse IgG (TBS 0.05% tween). The antibodies were incubated with the blotted membranes for 1 h at room-temperature or for overnight at 4°C. Proteins reacting with antibodies were detected with ECL Prime (Cytiva) and visualized with ChemiDoc Touch (BioRad). Acquired images were processed using Image Lab 6.1.0 (BioRad) and Photoshop 2023 (Adobe).

Immunofluorescence

For cKO-CENP-C DT40 cells expressing GFP-CENP-C, the cells were cytospun onto glass slides (Matsunami). The cells were fixed with 4% paraformaldehyde (PFA) in PHEM buffer (60 mM PIPES, 25 mM HEPES, 10 mM EGTA, 2 mM $MgCl_2$, pH 7.0 (NaOH)) for 10 min, permeabilized with 0.5% Triton X-100 in PHEM for 10 min, blocked with 0.5% BSA in PBS for 5 min and incubated with Cy3-labeled anti-chicken CENP-T[10] diluted with 0.5% BSA in PBS for 1 h at 37°C and then washed with 0.5% BSA in PBS 3 times. The cells were post-fixed with 4% PFA in PHEM for 10 min, washed with PBS and stained DNA with 100 ng/ml DAPI in PBS for 15 min. The stained samples were washed with PBS and mounted with VECTASHIELD Mounting Medium (Vector Laboratories).

For cKO-CENP-C DT40 cells expressing GFP-CENP-C and mScarlet-CENP-N or mScarlet-CENP-A, the cells were cytospun onto precision cover glasses (#1.5H Thickness, Thorlabs). The cells were fixed and permeabilized as above. After blocking with 0.5% BSA in PBS for 5 min, the cells were incubated with anti-chicken CENP-T[10] diluted with 0.5% BSA in PBS for overnight at 4°C. After 3-time washes with 0.5% BSA in PBS, the cells were incubated with Alexa Fluor 647-conjugated anti-rabbit IgG (Jackson ImmunoResearch) diluted with 0.5% BSA in PBS for 1 h at 37°C and then washed with 0.5% BSA in PBS 3 times. The cells were post-fixed with 4% PFA in PHEM for 10 min, washed with PBS, and stained DNA with 100 ng/ml DAPI in PBS for 15 min. The stained samples were washed with PBS and mounted with VECTASHIELD Mounting Medium (Vector Laboratories).

For RPE-1 immunofluorescence using spinning-disk confocal microscopy, RPE-1 cells were cultured on precision cover glasses (#1.5H Thickness, Thorlabs). The cells were fixed with 4% PFA in PHEM buffer for 10 min, permeabilized with 0.5% Triton X-100 in PHEM for 10 min, rinsed with 0.1% Triton X-100 in PBS, blocked with blocking solution (3% BSA, 0.1% Triton X-100, 0.1% NaN_3 in TBS) for 10 min, and then incubated with mouse anti-human CENP-A[79] diluted with blocking solution for overnight at 4°C. After 3-time washes with 0.1% Triton X-100 in PBS, the cells were incubated with Alexa Fluor 647-conjugated anti-mouse IgG (Jackson ImmunoResearch) diluted with blocking solution for 1 h at RT and then washed with 0.1% Triton X-100 in PBS 3 times. The cells were post-fixed with 4% PFA in PHEM for 10 min, washed with PBS, and stained DNA with 100 ng/ml DAPI in PBS for 15 min. The stained samples were washed with PBS and mounted with VECTASHIELD Mounting Medium (Vector Laboratories).

For RPE-1 immunofluorescence using STORM or MINFLUX nanoscopy, RPE-1 cells were prepared and fixed as above. The cells were stained with anti-human CENP-A together with rabbit anti-human Cyclin B1 (Cell Signaling Technology) as a mitotic cell marker. The anti-human Cyclin B1 was also diluted with blocking solution. The cells were incubated with antibodies for overnight at 4°C. After 3-time washes with 0.1% Triton X-100 in PBS, the cells were incubated with Alexa Fluor 647-conjugated anti-mouse IgG (Jackson ImmunoResearch) and Cy3-conjugated anti-rabbit IgG (Jackson ImmunoResearch) diluted with blocking solution for 1 h at RT and then washed with 0.1% Triton X-100 in PBS 3 times. The cells were post-fixed with 4% PFA in PHEM for 10 min, washed with PBS and stained DNA with 20 μM NucleoSeeing (Funakoshi) in PBS for 15 min. The samples were stored in PBS at 4°C for STORM and MINFLUX nanoscopy analysis.

Spinning-disk confocal microscopy

Immunofluorescence images were acquired at 0.2 μm intervals in the z-axis using a Zyla 4.2 sCMOS camera (Andor) mounted on a Nikon Ti inverted microscope with an objective lens (Nikon; Plan Apo lambda 100x/1.45 NA) with a spinning-disk confocal unit (CSU-W1, Yokogawa) controlled with NIS-elements AR 4.8 (Nikon) at RT. The images in the figures are the maximum intensity projection of the Z-stack generated with Fiji.[82] Acquired images were processed using Fiji[82] and Photoshop 2023 (Adobe).

Quantification of fluorescence signals on mitotic centromeres

The fluorescence signal intensities of GFP-CENP-C, mScarlet-CENP-N, or mScarlet-CENP-A co-localized with CENP-T on mitotic centromeres in DT40 cells were quantified using the Imaris software (Bitplane). To measure the immunostained CENP-T signals, the CENP-T signals co-localized with mScarlet-CENP-N on mitotic centromere in DT40 cells were quantified using the Imaris software (Bitplane). The fluorescence signals on about 50-100 centromeres in each of 10 mitotic cells were quantified and subtracted with the mean of background signals in non-centromeric regions in each cell and the mean value of the signals in each cell was calculated. Data are shown as Mean ± standard deviation using GraphPad Prims7 (GraphPad software). The unpaired t-test (two-tailed) was used. A p-value less than 0.05 is considered statistically significant.

The fluorescence signal intensities of GFP-hCENP-C co-localized with CENP-A on mitotic centromeres in RPE-1 cells were quantified using the Imaris software (Bitplane). The fluorescence signals on about 70 centromeres in each of 10 mitotic cells were quantified and subtracted with the mean of background signals in non-centromeric regions in each cell and the mean value of the signals in each cell was calculated. Data are shown as Mean ± standard deviation using GraphPad Prims7. The unpaired t-test (two-tailed) was used. A p-value less than 0.05 is considered statistically significant.

Chromosome alignment assay

cKO-CENP-C/mScarlet-CENP-A cells or those cells expressing GFP-CENP-C^{FL} or GFP-Mini-CENP-C were cultured in DT40 culture medium with Tet. At 44 h after Tet addition, MG132 (final 10 μM) was added into the culture, and the cells were further cultured for 4 h, and cytospun onto precision cover glasses (#1.5H Thickness, Thorlabs). The cells were fixed and permeabilized as above. Their DNA was stained with 100 ng/ml DAPI in PBS for 15 min. The stained samples were washed with PBS and mounted with VECTASHIELD Mounting Medium (Vector Laboratories). The mitotic cell images were acquired by the spinning-disc confocal microscopy as above. The XY-coordination of centromeres in a mitotic cell was determined as the center of each mScarlet-CENP-A spot using the Imaris software (Bitplane) and plotted to a two-dimensional plane. The consequent scatter plot was analyzed by confidence ellipses according to the Real Statistics Using Excel (www.real-statistics.com). The chromosome alignment was evaluated with the ratio of the semi-major axis to semi-minor axis of the ellipse; The length of the semi-major axis was divided by the length of the semi-minor axis and 1 was subtracted from the value (alignment value). About 70-100 centromeres in each of 20 mitotic cells were analyzed and the mean alignment value in each cell was calculated. Data are shown as Mean ± standard deviation using GraphPad Prims7 (GraphPad software). The unpaired t-test (two-tailed) was used. A p-value less than 0.05 is considered statistically significant.

Flow cytometry analysis

Ten ml of DT40 cell culture (5x10^6 cells/ml) was labeled with 20 μM BrdU (5-bromo-2'-deoxyuridine) for 20 min and harvested. The cells were washed with 10 ml ice-cold PBS, gently suspended with 13 ml 70% ethanol, and stored at –20°C. Following a wash with 1 ml 1% BSA in PBS, the cells were incubated in 1 ml 4 N HCl with 0.5% Triton X-100 for 30 min at RT and washed with 1 ml 1% BSA in PBS 3 times. The cells were incubated with 30 μl anti-BrdU (BD) for 1 h at RT, washed with 1 ml 1% BSA in PBS twice, incubated with 30 μl FITC-labeled anti-mouse IgG (Jackson ImmunoResearch, 1/20 in 1% BSA in PBS) for 30 min at RT, washed with 1 ml 1% BSA in PBS and stained DNA with 1 ml propidium iodide (10 μg/ml) in 1% BSA in PBS for overnight at 4°C. The stained cells were applied to Guava easyCyte (Merck). Obtained data were analyzed with InCyte software (Merck).

Protein expression and purification

E. coli cells (Rosetta2(DE3), Novagen) were transformed with pGEX-6P-1-CENP-C$^{C\text{-}term}$ to express chicken CENP-C$^{C\text{-}term}$ as a glutathione-S-transferase (GST)-fused recombinant protein. Cells were grown at 37°C until OD600 reached 0.6; protein expression was induced by addition of IPTG to a final concentration of 0.2 mM, and culture was continued for overnight at 17°C. Cells were harvested by centrifugation. The cell pellet was resuspended in buffer A (20 mM HEPES-NaOH pH 7.5, 500 mM NaCl, 5% Glycerol and 2 mM tris(2-carboxyethyl)phosphine (TCEP) and lysed by sonication on ice. The lysate was clarified by centrifugation and applied to a glutathione sepharose 4FF column (Cytiva) pre-equilibrated with buffer A. After extensive column washing with buffer A containing 1 M NaCl, the tag-free protein was eluted from the column by the GST-tag cleavage with human rhinovirus 3C (HRV3C) protease. The CENP-C$^{C\text{-}term}$ fragment was applied to a HiTrap SP HP cation exchange column (Cytiva), eluted with a linear NaCl gradient from 100 mM to 750 mM, and further purified by size-exclusion chromatography using HiLoad Superdex 16/60 200 pg column (Cytiva) in a buffer containing 20 mM HEPES-NaOH pH 7.5, 500 mM NaCl and 2 mM TCEP. Peak fractions containing the Cupin domain were combined, concentrated (typically to 8-10 mg/ml), and stored at -80°C until further use for crystallization and biochemical assay. CENP-C^{CBD}, Mini-CENP-C and Mif2p$^{C\text{-}term}$ were each expressed in *E. coli* cells (Rosetta2(DE3), Novagen) as a GST fusion protein. Mini-CENP-C or Mif2p$^{C\text{-}term}$ was prepared in the same way as the wild-type CENP-C$^{C\text{-}term}$. CENP-C^{CBD} was purified using GST affinity purification followed by the GST-tag cleavage and size-exclusion column chromatography. Bacterial expression and purification of CENP-C$^{677\text{-}864}$ F756P/757P (CENP-C$^{C\text{-}term\ pp}$) was performed in the same manner as wild-type CENP-C$^{C\text{-}term}$, but 0.1% Triton X100 was supplemented in buffer A only during lysate preparation.

GST-fused hCENP-C$^{C\text{-}term}$ or hCENP-C$^{C\text{-}term\Delta OI}$ was expressed in *E. coli* cells (Rosetta2(DE3), Novagen), lysed and purified by glutathione affinity column chromatography in the same manner to GST-fused chicken CENP-C$^{C\text{-}term}$. After the GST tag cleavage with HRV3C protease, the hCENP-C$^{C\text{-}term}$ or hCENP-C$^{C\text{-}term\Delta OI}$ fragment was purified using a HiTrap SP HP cation exchange column (Cytiva) with a linear NaCl gradient from 75 mM to 850 mM for elution. The peak fractions containing the hCENP-C fragment was further purified by size-exclusion chromatography using HiLoad Superdex 16/60 200 pg column (Cytiva) in a buffer containing 20 mM HEPES-NaOH pH 7.5, 300 mM NaCl, 5% Glycerol and 2 mM dithiothreitol (DTT). Peak fractions containing the hCENP-C$^{C\text{-}term}$ or hCENP-C$^{C\text{-}term\Delta OI}$ were combined and concentrated (2 mg/ml of hCENP-C$^{C\text{-}term}$, 4 mg/ml of hCENP-C$^{C\text{-}term\Delta OI}$).

E. coli cells (Rosetta2(DE3), Novagen) were transformed with pRSFDuet-MBP-CENP-N$^{C\text{-}term}$-MBP-CENP-L to express the chicken CENP-L-N complex as MBP-fused recombinant proteins (MBP-CENP-L/MBP-CENP-N$^{C\text{-}term}$, MBP-CENP-L-N). Cells were grown at 37°C until OD600 reached 0.6; protein expression was induced by addition of IPTG to a final concentration of 0.2 mM, and culture was continued for overnight at 17°C. Cells were harvested by centrifugation. The cell pellet was resuspended in buffer A and lysed by sonication on ice. The lysate was clarified by centrifugation, applied to amylose resin (New England BioLabs) pre-equilibrated with buffer A. The MBP-CENP-L-N complex was eluted with 20 mM maltose in buffer A, concentrated and purified by size-exclusion chromatography using HiLoad Superdex 16/60 200 pg column (Cytiva) in a buffer containing 20 mM HEPES-NaOH pH 7.5, 300 mM NaCl and 2 mM TCEP. Peak fractions containing the MBP-CENP-L-N complex were combined and concentrated (14 mg/ml).

MBP-AviTag-His6 was expressed in *E.coli* cells (Rosetta2 (DE3), Novagen) and lysed in 20 mM HEPES-NaOH pH 7.5 buffer containing 200 mM NaCl (MBP affinity buffer) using sonication on ice. The lysate was clarified by centrifugation and applied to amylose

resin (New England BioLabs). MBP-AviTag-His6 was eluted with 20 mM maltose in MBP affinity buffer. The elution was applied to a HiTrap Q HP anion exchange column (Cytiva) and eluted with a linear NaCl gradient from 50 mM to 750 mM. The peak fractions were combined and concentrated.

All the protein purification steps were performed at 4°C.

Crystallization and structural determination

Crystallization of the chicken CENP-C$^{C\text{-}term}$ was performed using the sitting-drop vapor diffusion method at 20°C. Octahedral crystals were grown from drops consisting of 200 nl of protein solution (10.4 mg/ml) and 100 nl of reservoir solution containing 0.2 M lithium citrate, 0.1 M MES-NaOH pH 6.5 and 20% PEG4000. For X-ray diffraction measurements, the crystals were cryoprotected in reservoir solution supplemented with 20% Glycerol. X-ray diffraction datasets were collected at 100 K on the synchrotron beamline BL-26B1 at SPring8 (Himeji, Japan). Diffraction data were processed using XDS.[84] Data collection statistics are summarized in Table S1. The structure of the chicken CENP-C Cupin domain was determined by the molecular replacement method using Molrep[85] in the CCP4 suite.[86] The coordinates of the *Saccharomyces cerevisiae* Mif2p Cupin domain (PDB: 2VPV) were used as a search model. The initial model was built using Coot.[87] Structural refinement was conducted using REFMAC.[88] The final model containing residues 722-850 was built by iterative reciprocal space refinement and manual rebuilding. The statistics of structural refinement and the quality of the final model are summarized in Table S1. Secondary structure assignment was performed using DSSP.[89] Molecular graphics and analyses were performed with UCSF ChimeraX.[95] All figures depicting the crystal structure in Figure S2B were produced using the PyMOL molecular graphics system (Schrödinger, LLC).

Blue native-polyacrylamide gel electrophoresis (PAGE)

Eight to ten micrograms of purified chicken CENP-C$^{C\text{-}term}$, chicken CENP-C$^{C\text{-}term\ PP}$, hCENP-C$^{C\text{-}term}$, hCENP-C$^{C\text{-}term\Delta OI}$ or Mif2p$^{C\text{-}term}$ were dissolved in 5 μl Native PAGE sample buffer (50 mM Tris-HCl pH 7.5, 10% Glycerol, 50 mM NaCl, 0.001% Ponceau S, 0.5% Coomassie G-250) and applied to a 10%–20% gradient gel (NativePAGE Bis-Tris gel; Thermo Fisher Scientific) and migrated at 150 V for 180 min at 4°C. Native PAGE running buffer (50 mM Bis-Tris, 50 mM Tricine, pH 6.8) was used as a positive electrode and Native PAGE running buffer supplemented with 0.02% Coomassie G-250 was used as a negative electrode. The bands were visualized by destaining the gel with water.

In vitro pulldown assay

Fifty picomoles of the MBP-CENP-L/CENP-N$^{C\text{-}term}$ complex (MBP-CENP-L-N) or MBP-AviTag-His6 (MBP) were added to 5 μl (bed vol.) MBP-Trap agarose beads (Proteintech) in 25 μl pulldown buffer (20 mM HEPES-NaOH, pH7.4, 200 mM NaCl, 5% Glycerol, 1 mM DTT, 0.05% NP40) and incubated for 1 h on ice with gentle mixing. The MBP-CENP-L-N or MBP-bound beads were washed with pulldown buffer 3 times and incubated with 200 pmole CENP-C^{CBD}, CENP-C$^{C\text{-}term}$, or Mini-CENP-C in 50 μl pulldown buffer for 1 h on ice with gentle mixing. The beads were washed with 200 μl pulldown buffer 3 times. The proteins were eluted with 10 μl 1xLSB and heated for 5 min at 96°C. The samples were run on 12.5% SDS-PAGE (Input: 50 pmole of each protein, Pulldown: all eluted proteins of each sample) and stained with Brilliant Blue R (Sigma). The band intensities of the input and pull-downed proteins on the SDS-PAGE were quantified by Image Lab 6.1.0 (BioRad). To examine the CENP-C protein amount pull-downed by MBP-CENP-L-N, the band intensities of pull-downed CENP-C were adjusted by the molecular weight of each CENP-C protein and normalized by the band intensities of the pull-downed CENP-N$^{C\text{-}term}$. Because there is a contaminant protein in MBP-CENP-L-N that migrated to the same size as the Mini-CENP-C, the contaminant intensity value was subtracted from the Mini-CENP-C intensity value. The results of three independent experiments were analyzed and the relative amount of each pull-downed CENP-C was calculated. Data are shown as Mean ± standard deviation using GraphPad Prims7 (GraphPad software). The unpaired t-test (two-tailed) was used. A p-value less than 0.05 is considered statistically significant.

2D-STORM

The immunostained RPE-1 cells on the cover glass were mounted with freshly prepared oxygen scavenger imaging buffer (50 mM Tris-HCl pH 8.0, 10 mM NaCl, 10% Glucose, 0.7 μg/μL Glucose Oxidase (Sigma, #G2133-250KU), 0.04 μg/μL Catalase (FUJIFILM, #035-12903) and 70 mM 2-mercaptoethanol) based on the glucose oxidase enzymatic system (GLOX) for STORM using a frame-sealed incubation chamber (Bio-Rad). 2D-STORM acquisitions were performed using a Nikon N-STORM with Eclipse Ti-E inverted microscope and laser TIRF illuminator (Nikon Instruments Inc.). Alexa 647 fluorophores were stochastically excited using the 640 nm laser beam with an additional 405 nm weak pulse. Images were acquired with an Andor iXon 897 EMCCD camera (Andor Technologies) and a CFI Apo TIRF 100× objective lens (N.A. 1.49). For each cell, a stack of 10,000 frames was acquired at an exposure time of 16 ms and information including the XY coordinates of the detected blinking spots was extracted using Nikon NIS-Element imaging software (Nikon Instruments Inc.).

MINFLUX nanoscopy

For the stabilization process during MINFLUX measurements, the immunostained RPE-1 cells as above were incubated for 5-10 min with an undiluted dispersion of 150 nm gold beads (EM.GC150/4, BBI Solutions). After washing with PBS, the samples were mounted with GLOX+MEA imaging buffer (50 mM Tris-HCl, 10 mM NaCl, 10% (w/v) Glucose, 64 μg/ml catalase, 0.4 mg/ml glucose oxidase,

25-30 mM MEA, pH 8.0).[96] The MINFLUX measurements and the corresponding confocal images were acquired with an abberior MINFLUX (Abberior Instruments GmbH) equipped with a 642 nm (CW) excitation laser for confocal and MINFLUX imaging, a 488 (CW) excitation laser for confocal imaging and a 405-nm (CW) laser for activation. The 642 nm beam was shaped using a spatial light modulator. The EOD-based MINFLUX scanning was performed as described before.[97] A 60x magnification 1.42 NA oil objective lens (UPLXAPO60XO, Olympus) was used for all measurements. The emission upon 640 nm excitation was detected on two avalanche photodiodes with fluorescence filters from 650 to 780 nm. The fluorescence emitted at 488 nm excitation was counted on an avalanche photodiode with a fluorescence filter from 500 to 620 nm. To stabilize the sample during MINFLUX measurements, a reflection-based stabilization system with a 980 nm laser was applied.[97]

Rendering 2D-STORM and MINFLUX images

Two-dimensional single-molecule localization microscopy data mainly consists of the localization coordinates (x_n,y_n), the intensity I_n, and the lateral localization accuracy σ_n for the nth blinking dot: $\{(x_n, y_n, I_n, \sigma_n)\}_{n=1}^{N}$. Then, we calculated the total intensity by

$$I_{\text{total}}(x,y) = \sum_{n=1}^{N} \frac{I_n}{2\pi\sigma_n^2} \exp\left(- \frac{(x - x_n)^2 + (y - y_n)^2}{2\sigma_n^2} \right),$$

and mapped it on a pixel region with the Gaussian filter for smoothing. Here, we developed the rendering algorithm as Python code. In MINFLUX, since the localization precision needs to be determined empirically via the spread of the localizations on each trace,[97] we set $\sigma_n = 2$ nm.

Pair correlation analysis

First, to crop appropriate clusters of dots of fluorophore emitters labeling CENP-A molecules, we applied the density-based clustering algorithm DBSCAN (Density-Based Spatial Clustering of Applications with Noise). We set the main two parameters *eps* = 100 nm, which is the maximum distance between two dots for one to be considered to be connected to the other, and *minPts* = 5, the minimum point number in a neighborhood for a dot to be considered as a core dot.

Then we calculated the normalized pair correlation function for each cropped localization coordinate data $\{(x_{n,i}, y_{n,i})\}_{n=1}^{N_i}$ of the *i*th cluster in the cropped rectangular region. In principle, the pair correlation function for randomly distributed dots reveals the unit value. However, the pair correlation function for dots in a cropped region inevitably includes the boundary effect. In order to eliminate the boundary effect, we numerically prepared uniformly distributed N_i dots in the same rectangle region for the *i*th cluster. Based on the pair-wise Euclidean distance between dot *n* and *m*, r_{nm}, we calculated the histogram $h_{\text{cluster}}(r)$ and $h_{\text{random}}(r)$ of the distance for both clustered and random dots with the 2-nm binning width. For smoothing $h_{\text{random}}(r)$, we prepared 100 sets of random dots and averaged these histograms. Finally, the normalized pair correlation function was calculated by: $g(r) = h_{\text{cluster}}(r)/h_{\text{random}}(r)$ (Figure S7C). From this definition, when the normalized pair correlation function curve monotonically decays from $r = 0$ with $g(r) > 1$ and crosses $g(r) = 1$, we can state that the dots are clustering within the distance for $g(r) > 1$. Therefore, the distance satisfying $g(r) = 1$ can be a characteristic length of the clustering dots.

3C-qPCR

The ligation frequencies within the centromeric chromatin were measured by chromosome conformation capture (3C)-qPCR[58] with several modifications to optimize for the centromeric chromatin in DT40 cells.

- Crosslinking and lysis

DT40 cells (1x10^7 cells) were suspended in 10 ml fresh DT40 culture medium and crosslinked by adding final 1% PFA (16%, Electron Microscopy Sciences). After 10 min at RT, the cells were moved onto ice and added final 0.2 mM Glycine to quench the crosslinking reaction. The reaction mixture was centrifuged for 5 min at 220 x *g* at 4°C and the supernatant was aspirated. The cell pellets were washed with 10 ml ice-cold PBS twice. After centrifugation for 5 min at 220 x *g* at 4°C, the supernatant was aspirated, and the cell pellets were resuspended in 5 ml lysis buffer (10 mM Tris-HCl pH 7.5, 10 mM NaCl, 0.2% NP-40, 1x complete EDTA-free proteinase inhibitor (Roche)) and incubated for 15 min on ice. The mixture was centrifuged for 5 min at 400 x *g* at 4°C, and the supernatant was aspirated. The cell pellets were resuspended with 5 ml lysis buffer, centrifuged for 5 min at 400 x *g* at 4°C, and the supernatant was aspirated.

- Restriction enzyme digestion and ligation

The precipitates were resuspended and transferred into a new 1.5 ml tube with 0.5 ml 1.2 x restriction enzyme B-buffer (Nippon Gene). Seven point five microliters of 20% (w/v) SDS (final 0.3%) were added into the suspension. The reaction mixture was incubated for 1 h at 37°C with shaking at 900 rpm. Following 50 μl 20% (v/v) Triton X-100 addition (final 2%), the mixture was incubated for 1 h at 37°C with shaking at 900 rpm. Four hundred and eighty units of HindIII (4 μl of 120 U/μl, Nipone Gene) was added into the reaction and incubated for overnight at 37°C with shaking at 900 rpm. After addition of 40 μl 20% (w/v) SDS (final 1.6%), the mixture was incubated for 20 min at 65°C. The reaction mixture was transferred to 50 ml tube, diluted with 6.125 ml 1.15 x ligation

buffer (1 x ligation buffer: 60 mM Tris-HCl pH 7.5, 5 mM DTT, 5 mM $MgCl_2$, 1 mM ATP) and supplemented with 375 μl 20% Triton X-100 (final 1%). The mixture was incubated for 1 h at 37°C with shaking at 180 rpm. Five microliters of 20 U/μl T4 ligase (Promega) were added into the mixture and incubated for 4 h at 16°C, followed by further incubation for 30 min at RT. The reaction mixture was digested by adding 15 μl 20 mg/ml Proteinase K and incubation for overnight at 65°C. Digestion efficiency of samples was assessed following Hagège et al.[58]

-DNA purification

Thirty microliters of 10 mg/ml RNase A were added to the reaction mixture and incubated for 30 min at 37°C. The digested sample was mixed with 7 ml Phenol/Chloroform/Isoamyl alcohol (25:24:1, Nippon Gene) and centrifuged for 15 min at RT at 2,200 x *g*. The aqueous phase was transferred to a new tube, mixed with 7 ml Chloroform and centrifuged for 15 min at RT at 2,200 x *g*. The aqueous phase was transferred to a new tube, mixed with 700 μl sodium acetate and 17. 5 ml ethanol and placed at -80°C for overnight. The mixture was centrifuged for 15 min at 4°C at 2,200 x *g*. After removal of supernatant, ten milliliters of 70% ethanol were added into the tube and centrifuged for 15 min at 4°C at 2,200 x *g*. The supernatant was discarded. The pellets were briefly dried at RT, then dissolved in 150 μl 10 mM Tris-HCl pH 7.5 and transferred into a new 1.5 ml tube.

-Secondary restriction enzyme digestion

The purified DNA was mixed with 25 μl H_2O, 20 μl 10x restriction enzyme H-buffer (Nippon Gene) and 5 μl 20 U/μl EcoRI (final 100 U, Nippon Gene), and incubated for 2 h at 37°C. The digested sample was mixed with 200 μl Phenol/Chloroform/Isoamyl alcohol (25:24:1, Nippon Gene) and centrifuged for 5 min at RT at 16,000 x *g*. The aqueous phase was transferred to a new tube, mixed with 200 μl Chloroform and centrifuged for 5 min at RT at 16,000 x *g*. The aqueous phase was transferred to a new tube, mixed with 20 μl sodium acetate and 0.5 ml ethanol and placed at -80°C for overnight. The mixture was centrifuged for 5 min at 4°C at 16,000 x *g*. After removal of supernatant, half a milliliter of 70% ethanol was added into the tube and centrifuged for 5 min at 4°C at 16,000 x *g*. The supernatant was discarded. The pellets were briefly dried at RT and then dissolved in 50 μl 10 mM Tris-HCl pH 7.5. After measuring DNA concentration using Qubit dsDNA HS Assay Kit (Thermo Fisher Scientific), the 3C library was stored at -80°C.

-TaqMan qPCR

TaqMan MGB (5'-FAM) probes for the native centromere of the Z chromosome and the neo-centromere on the Z chromosome were designed and synthesized at Thermo Fisher Scientific. For loading control, a TaqMan MGB (5'-FAM) probe for SMC5 locus on the Z chromosome was also designed and synthesized at Thermo Fisher Scientific. Fifty nanograms of DNA template (3C library) were mixed with TaqMan qPCR reaction mixture: 900 nM constant primer, 900 nM test primer, 250 nM TaqMan probe in 10 μl 1x TaqMan Fast Advanced Master Mix (Thermo Fisher Scientific). qPCR was performed on QuantStadio 3 (Thermo Fisher Scientific) with the following cycling condition: 2 min at 95°C, 40 cycles of 1 s at 95°C, and 20 s at 60°C. To make a standard curve, a plasmid, which contained the ligated chimeric DNA fragment corresponding to each target site was serially diluted and used for qPCR analysis. All samples were run in triplicate and the mean value of the triplicates was calculated. The slope (a) and *y*-intercept (b) values were determined from the standard curve for each experiment. The ligation frequency values were calculated as follows: $v=10^{(Ct-b)/a}$. The values were normalized with the loading control value ($v_{smc5}=10^{(meanCt-b)/a}$) of each 3C library to obtain the relative ligation frequencies.

QUANTIFICATION AND STATISTICAL ANALYSIS

Details regarding quantification and statistical analysis can be found in the corresponding figure legends and Experiment Details section of the STAR Methods.